WATER RESOURCES RESEARCH, VOL. 31, NO. 3, PAGES 601–618, MARCH 1995

# A model for deuterium and oxygen 18 isotope changes during evergreen interception of snowfall

H. C. Claassen and J. S. Downey

Water Resources Division, U.S. Geological Survey, Denver, Colorado

**Abstract.** A one-dimensional, physically based numerical model was constructed to describe the isotopic enrichment observed in throughfall of snow intercepted on evergreens. The process of enrichment is similar to that which results in formation of depth hoar in snowpack. On-site data were obtained at a high-altitude (3500 m) watershed in the Colorado Rocky Mountains. The model includes the ambient atmospheric variables of temperature, relative humidity, and water vapor isotopic composition and the intercepted snow variables of temperature profile, permeability for viscous flux, and isotopic composition. Model simulations yield results similar to those observed on site and suggest that the process is dominated by diffusive flux despite the very high permeability of freshly fallen snow. Median enrichments were observed to be 2.1‰ in oxygen 18 and 13‰ in deuterium.

## Introduction

Isotopic enrichment of evaporating water has been described by *Craig et al.* [1963], *Craig and Gordon* [1965], *Merlivat and Coantic* [1975], and *Stewart* [1975]. These studies indicate the importance of turbulent transfer from the water surface, water vapor pressure and isotopic composition of the atmosphere, and the possible effect of liquid phase diffusion in determining the final composition of the liquid.

The nature of snow as a porous medium, in contrast to liquid water, imposes significant constraints on application of water isotope enrichment models to this medium. Some of the variables that affect evaporating liquid, in which constant temperature is assumed to prevail, have minimal effect on the isotopic composition of remaining snow, primarily because of the temperature gradients in the snow. These gradients result in transfer of vapor in snow pore space from regions of higher vapor pressure (higher temperature) to regions of lower vapor pressure (lower temperature) where condensation occurs [*Seligman*, 1936; *Bader et al.*, 1939; *Schytt*, 1958; *Epstein et al.*, 1965; *Gow*, 1965; *Trabant and Benson*, 1972; *Whillans and Grootes*, 1985; *Sommerfeld et al.*, 1991; *Friedman et al.*, 1991]. In addition to intrasnow vapor transfer, loss of snow by sublimation occurs at the surface of a body (the porous snow) that cannot be assumed mixed (or of constant composition) throughout the process. In evaporation of water the potential for maintaining the fluid surface nearer its original composition exists by virtue of viscous flow and diffusion in the liquid. In evaporation of snow, however, the initial vapor associated with the snow may be the equilibrium vapor, but over a short time the vapor released by the snow should approach the composition of the solid. This must be true because isotope gradients cannot be formed in the solid phase during periods of time the snow is held on the tree branches, generally hours to a few days. Although the model presented here assumes that vapor released from the snow maintains the average composition of the snow, other assumptions regarding the isotopic composition of the vapor do not change the model formulation.

One aspect of interception of snowfall by evergreens that affects the final isotopic composition is the large increase in surface area of snow exposed to evaporation over that which is formed when snow falls on the ground surface. This results in higher energy absorption, and hence evaporation, for a given water equivalent of precipitation. In a forested watershed, dense evergreen growth may cause over one-half the precipitation to be lost to evaporation [*Hoover and Leaf*, 1967; *Troendle and King*, 1985; *Claassen et al.*, 1986]. Isotopic modification of the remaining snow could have a significant effect on the isotopic composition of water available for groundwater recharge, resulting in modified interpretation of groundwater isotope data in water balance and paleoclimate studies.

Measurements made at Snowshoe Mountain, a Rocky Mountain watershed near Creede, Colorado, have shown that significant enrichment in water isotopes HDO and $H_2{}^{18}O$ occurs while snowfall is intercepted by evergreens. This paper describes these measurements and presents a model of the process.

## Description of Study Area

In a long-term study of water, water isotope, and solute transport, measurements of isotopic composition of incident precipitation and evergreen throughfall have been made for several years at Snowshoe Mountain, located about 5 km south of Creede, Colorado. The throughfall measurements were made at a site near the summit, at an elevation of nearly 3500 m. The climate of the site can be characterized as being cool, having a mean annual temperature near freezing, and moderately wet, having an annual precipitation average of about 53 cm, more than one half of which falls as snow [*Bates and Henry*, 1928].

## On-Site Methods and Results

Monthly or quarterly integrated samples of incident precipitation and throughfall were obtained from 1981 to 1989 using a 40-cm-diameter cylinder with a less than 2-cm restriction to minimize evaporation or isotopic exchange with changing at-



Paper number 94WR01995.

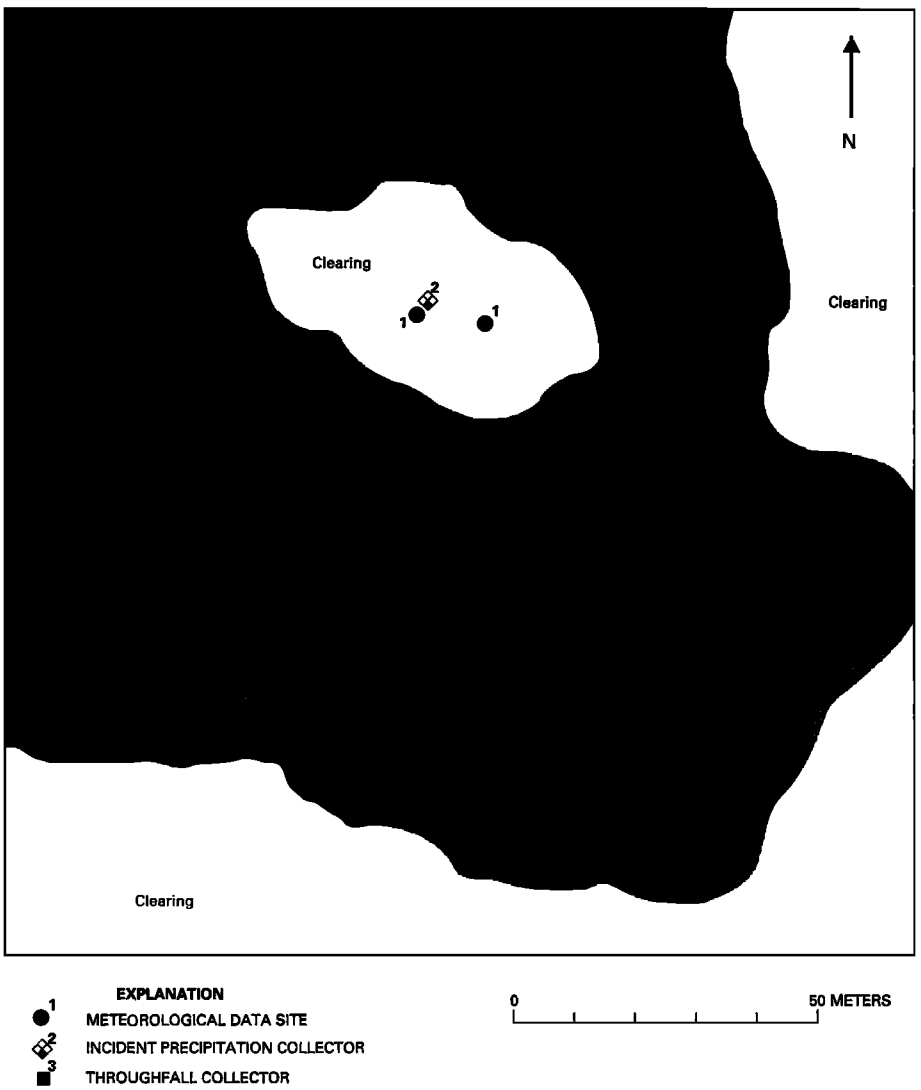


**Figure 1.** Plan view of throughfall collection site, Snowshoe Mountain, Colorado.

mospheric compositions. Comparison of precipitation amounts determined from sample volumes collected in the incident, open area collector with a U.S. standard rain gage shows the larger-diameter collector to be slightly more efficient than the rain gage, and evaporation losses, therefore, probably are minimal. The possibility of isotopic exchange between snow in the collectors and the atmospheric water vapor is more difficult to evaluate, but a simple study designed to evaluate the effect of exchange on water stored in this collector has shown insignificant impact. A plan view of the site is shown in Figure 1.

A summary of the data obtained is available on diskette.[1] It is evident from the data that about one-half the input precipitation is lost by interception (Figure 2). This occurs in summer (July–September) and winter (October–June). Only winter samples, however, display enrichment in the throughfall samples. The average difference between the isotopic composition of incident precipitation and throughfall for the period of record is $\Delta\delta D = 13‰$ and $\Delta\delta^{18}O = 2.1‰$. The corresponding average difference for the summer period is $\Delta\delta D = -0.19‰$ and $\Delta\delta^{18}O = 0.03‰$, within the estimated analytical accuracy ($2\sigma$) of $\delta D = 2‰$ and $\delta^{18}O = 0.2‰$. *Saxena* [1986, Table 1] reports similar results for pine forest throughfall in Sweden: precipitation loss of about 56% and a mean $\Delta\delta^{18}O = 0.25$, for 24 samples. It may be concluded that enrichment of samples occurs whenever the period of interception is relatively long, such as occurs during snowfall. Although no other observations of snow interception enrichment have been reported in the literature, *Judy et al.* [1970] and *Moser and Stichler* [1974] describe observations of enrichment in snowpack. Quantitatively, their observations show similar enrichment to ours. The observations of Moser and Stichler were followed by laboratory experiments that suggested the enrichment may be related

[1]An electronic supplement of this material may be obtained on a diskette or anonymous FTP from KOSMOS.AGU.ORG. (LOGIN to AGU's FTP account using ANONYMOUS as the user name and GUEST as the password. Go to the right directory by typing CD APEND. Type LS to see what files are available. Type GET and the name of the file to get it. Finally, type EXIT to leave the system.) (Paper 94WR01995, A model for deuterium and oxygen 18 isotope changes during evergreen interception of snowfall, by H. C. Claassen and J. S. Downey.) Diskette may be ordered from American Geophysical Union, 2000 Florida Avenue, N.W., Washington, DC 20009; $15.00. Payment must accompany order.

to vapor transport in snowpack resulting from temperature profiles that exist in a metamorphosing snowpack. In more recent work, *Friedman et al.* [1991] have studied enrichment of snowpack by depth hoar formation (Fairbanks, Alaska) and in experimental depth hoar formation [*Sommerfeld et al.*, 1991]. Other studies of snowpack isotopy have been done in polar regions [e.g., *Whillans and Grootes*, 1985]. It is reasonable to anticipate that this same process might be operating during interception.

The data also include values for the enrichment ratio ($\Delta\delta D/\Delta\delta^{18}O$) for each winter sample. Figure 3 summarizes these data in the form of a bar graph showing the frequency distribution of enrichment ratio, the most probable values lying between 4 and 8.

The probable importance of temperature gradients in intercepted snow prompted design of a device to measure the time-variable temperature profiles under typical interception conditions (Figure 4). This device consists of a stack of 0.4-mm-diameter thermistors encased in 1-mm × 13-mm glass housing. These were mounted on a 3-mm-diameter × 10-cm wood stalk that could be clamped to an evergreen branch. Spruce branches and needles form a more or less planar array that acts as an efficient platform for snow interception. Six thermistors were placed at 2-cm intervals, and the output was connected to a micrologger. Data collection was limited to periods of actual observation so the depth of snow on the branch could be noted. Typical examples of results are shown in Figures 5 and 6. These figures plot snapshots of intercepted snow temperature profiles taken at the times shown on the lower abscissa. Depths are shown on the upper abscissa, and the data points indicate the temperature profiles. The air temperature measurement is shown by the horizontal line. The steep temperature gradients that form after sunrise (Figure 6) and nightfall (Figure 5) should be noted. A further significant observation is that the interception period generally is terminated when the snow temperature rises to freezing, regardless of the air temperature (Figure 6, beginning at 1230 local time (LT)). A small amount of melting appears to lubricate the snow/leaf contact and allow the snow to slide off. Many on-site observations suggest that clear sky conditions, rather than wind or air temperature, provide energy to warm the snow and appear to be primary in determining interception residence time for appropriately oriented branchlets. The wide range in day-night air temperatures generates a similar wide range in snow temperatures (as shown in Figures 5 and 6, for example), but three general profile types may be recognized: symmetrical (e.g., December 24, 1988, 0700 LT), linear (e.g., December 24, 1988, 0300 LT), and step (e.g., December 30, 1988, 1130 LT). These are illustrated in Figure 7.

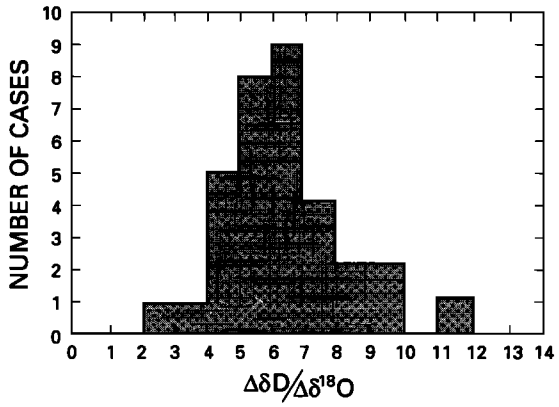


**Figure 3.** Frequency distribution of enrichment ratio values from throughfall at Snowshoe Mountain, Colorado.

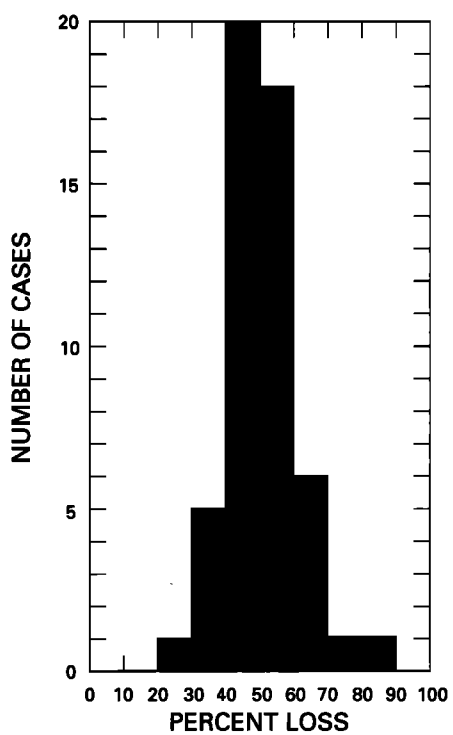


**Figure 2.** Distribution of precipitation loss resulting from interception of snow at Snowshoe Mountain, Colorado.

## Conceptual Model

Development of a model to simulate the processes resulting in isotope enrichment in intercepted snow requires knowledge of the pore structure of freshly fallen snow and changes that occur as the snow metamorphoses during the interception period, which may range from hours to several days. *Rogers* [1979], *Colbeck* [1980], and *Gray and Male* [1981], provide excellent summaries on the physics of snow formation, deposition, and metamorphosis. Unfortunately, details of the structure of snow that are pertinent to modeling gas transport in freshly fallen snow remain obscure [*Shimizu*, 1970; *de Quervain*, 1973; *DeHoff*, 1983; *Davis et al.*, 1987; *Dozier et al.*, 1987; *Sommerfeld and Rocchio*, 1989]. Therefore the following approach was used to model processes during snow interception on evergreens. The snow was assumed to consist of an infinite plate resting on an evergreen branch. The plate comprises a set of layers (cells) each of which has an associated temperature and water vapor pressure. Because this is an isotope model, the water vapor pressure is divided into partial pressures for each water isotope ($H_2{}^{16}O$, HDO, $H_2{}^{18}O$). The objective was to model vapor fluxes between cells and to or from the atmosphere, allow for condensation and evaporation, and compute a final composition of the remaining snow after varying periods of exposure. Both viscous and diffusive fluxes were considered, but it was determined that the viscous flux was less than 0.5% of the total flux for conditions expected at the Snowshoe Mountain site and was therefore minimal. The appendix de-

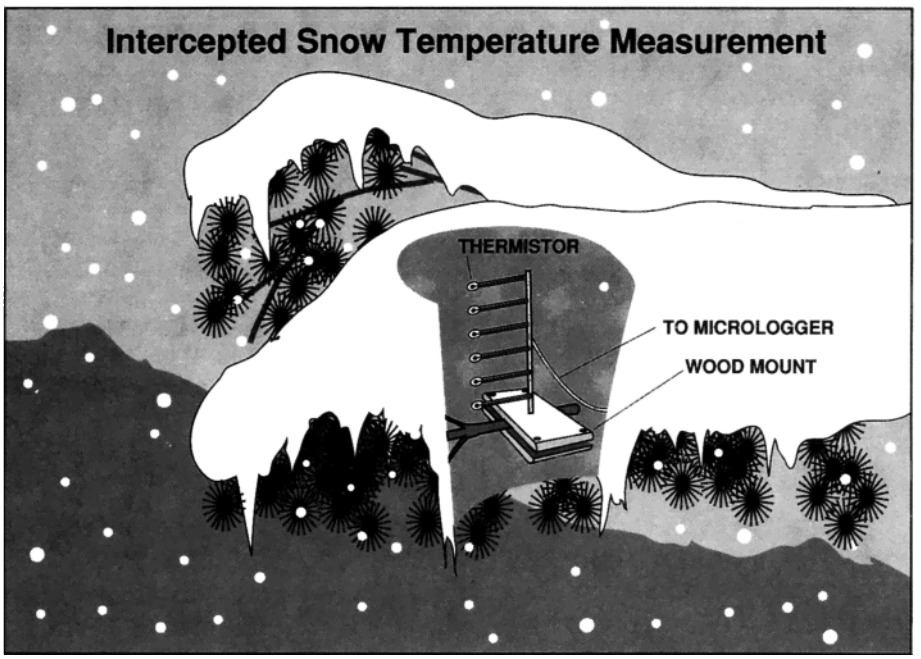


**Figure 4.** Diagram of intercepted snow temperature measurement.

scribes the methods used to estimate the relative amounts of diffusive and viscous flux.

Figure 8 shows a stack of unit cells that section the intercepted snowpack. A unit cell represents the void volume described by a unit area perpendicular to the vapor flux vector multiplied by the cell thickness, which may be varied to suit individual circumstances. The stack of cells represents void space only. We assume that voids account for more than 85% of the snowpack (fresh snow), that the snow does not impede gas flux, and that viscous flow to the atmosphere (and between cells) is minimal. The model also assumes that the supporting branchlets do not impede diffusion of vapor from the snowpack to the atmosphere.

The model uses a one-dimensional, steady state formulation to estimate the nonsteady viscous and diffusive flux between cell pairs and between cells delineating the snow boundaries and the atmosphere. Because condensation may occur in some cells, it cannot be assumed that a steady state vapor composition is reached during the period of time defined by snow interception. Therefore a time step must be chosen for which an instantaneous flux is representative. The fluxes between all cells are used to determine changes in vapor composition in each cell, taking into account condensation or vaporization necessary to maintain the equilibrium vapor pressure determined by cell temperature. Condensation follows rules for equilibrium isotope fractionation. Newly vaporized snow has the composition of the original snowfall. This is an important assumption: that all evaporated snow is original, not recondensed, vapor. This is a reasonable assumption for most situations because the predominant evaporation occurs from the upper (and lower) snow layers, where the vapor pressure gradients are largest. Clearly, the assumption loses validity as the fraction of snow lost increases and the recondensed vapor becomes the dominant fraction of remaining solid. It is important to recognize that this laminar flow model assumes that the only viscous flux is produced by pressure gradients arising from the diffusive fluxes present in the system. The possibility of viscous fluxes resulting from eddies developed by atmospheric turbulence cannot be dismissed, but on-site observations in dense evergreen forest suggest that mean wind speeds approach zero for much of the region below the canopy crown. This would not be true for lone trees, forests of low vegetation density, or trees at the edge of large clearings. Barometric pressure fluctuations can generate fluxes in snowpack on the ground [*Colbeck*, 1989], but intercepted snow is subject to pressure fluctuations on all sides and, therefore, little or no pressure gradients in the snow will be generated. As is commonly done in this type of modeling, results for each time step are summed to approximate the dynamic flux.

For each time step and each isotope ($H_2{}^{16}O$, HDO, $H_2{}^{18}O$), the model computes fluxes across each boundary and algebraically sums the fluxes to arrive at a net vapor composition change in a given cell. If the net change is less than zero, snow is vaporized to bring the total vapor pressure in that cell into equilibrium with the chosen conditions (generally, saturation equilibrium). If the vapor pressure exceeds equilibrium, an appropriate amount of vapor is condensed according to equilibrium condensation fractionation factors. This process is continued for each time step, with the isotopic composition of vapor condensed accumulated in a separate file. The isotopic composition of vapor lost to the atmosphere, if appropriate, is also accumulated in an additional computer file.

Values for certain variables required to effect the computations are obtained as follows.

Within the snow, $P_{H_2O} = \Sigma_i P_i$ where $P_{H_2O}$ is the total vapor pressure of water (all isotopes) and $P_i$ is the partial vapor pressure of each isotope $i$ (*Dorsey* [1940], as cited by *Eisenberg and Kauzmann* [1969]):

$$\log_{10} P_{H_2O(^{ice}_{eq})} = \left[ \frac{-2445.5646}{T} + 8.2312 \log_{10} T \right.$$

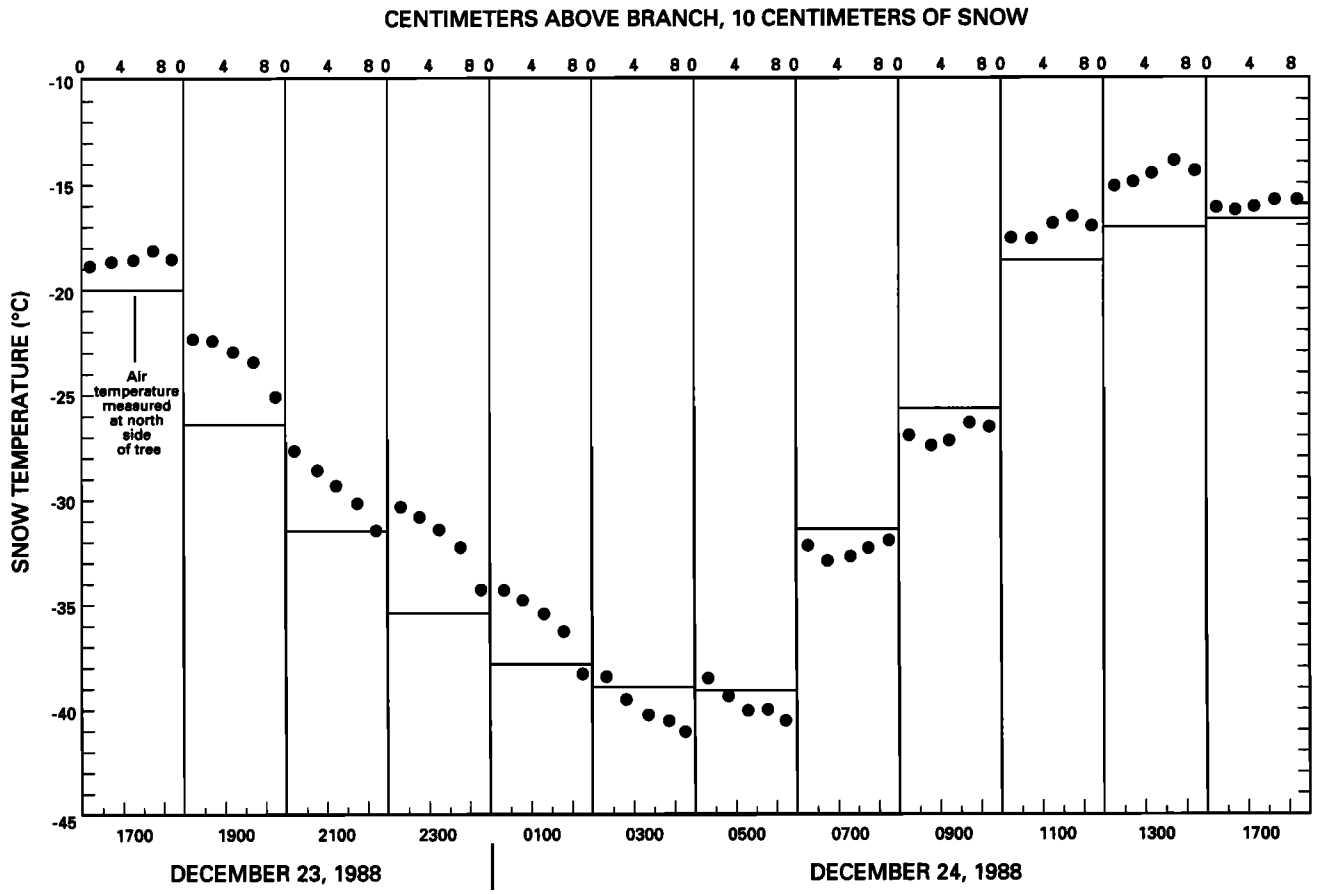


**Figure 5.** South facing branch temperature profiles, showing changes in temperature profile occurring during a diurnal cycle.

$$- 1677.006 \times 10^{-5}T + 120{,}514 \times 10^{-10}T^2 - 6.757169\left]\frac{1.01325 \times 10^6}{760}\right.$$

The equilibrium vapor pressure at $T$ (kelvins) is referenced to ice.

In the atmosphere,

$$P_{H_2O} = P_{H_2O(^{ice}_{eq})}RH$$

where RH is the relative humidity. Computationally, the pressures are converted to molecular concentrations for each water vapor isotope $C_i$, the values being a function of either the input isotope composition of the atmosphere or the vapor inside the snow:

$$C_i = [P_{H_2O}N_{AV}/RT][1 + R_{SMOW\ HDO} + R_{SMOW\ H_2{}^{18}O} + R_{SMOW\ HDO}(\delta D/1000) + R_{SMOW\ H_2{}^{18}O}(\delta^{18}O/1000)]^{-1}$$

where $N_{AV}$ is Avogadro's number ($6.02 \times 10^{23}$), $R$ is the gas constant, and the various subscripted $R$ terms are defined in the notation section. Specifically [*Fritz and Fontes*, 1980, pp. 11–13],

$$C_{H_2{}^{16}O} = \frac{P_{H_2O}}{T}\left[\frac{6.023 \times 10^{23}}{8.314 \times 10^7}\right] \cdot \left[\frac{1}{1.00216096 + 1.5576 \times 10^{-7}\delta D + 2.0052 \times 10^{-6}\delta^{18}O}\right]$$

$$C_{HDO} = C_{H_2{}^{16}O}[1.5576 \times 10^{-4}]\left[1 + \frac{\delta D}{1000}\right]$$

$$C_{H_2{}^{18}O} = C_{H_2{}^{16}O}[2.0052 \times 10^{-3}]\left[1 + \frac{\delta^{18}O}{1000}\right]$$

Air diffusivity $D_{AIR/i}$ of each isotope is

$$D_{H_2{}^{16}O} = 0.00127T_{AV} - 0.12731$$

$$D_{HDO} = 0.00127T_{AV} - 0.13449$$

$$D_{H_2{}^{18}O} = 0.00127T_{AV} - 0.13319$$

where $T_{AV}$ represents the absolute temperature average between each adjacent pair of cells.

The temperature dependence of the diffusivity was determined by partial differentiation with respect to $T$ of the simplified relation for $D$ derived from kinetic theory (as given, for example, by *Merlivat* [1978, equation (15)]). Temperature dependence of diffusivity for water/air also was calculated using equation 16.4–13 of *Bird et al.* [1960, p. 505]. The calculated values were in substantial agreement (0.00122) with values

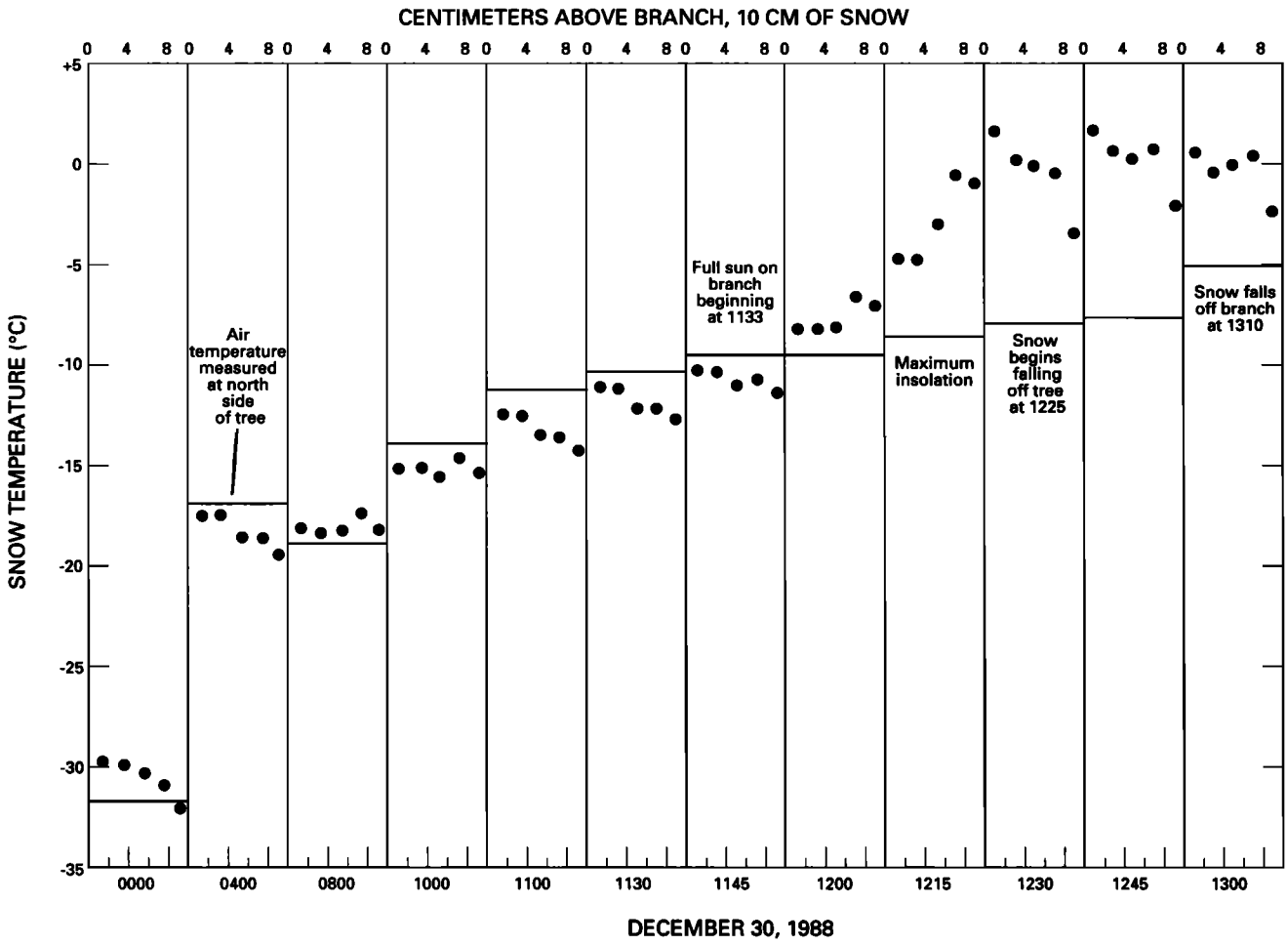


**Figure 6.** East facing branch temperature profiles, showing changes in temperature profile occurring during a semidiurnal cycle.

given above. Values for $D_{H_2O}$, $D_{HDO}/D_{H_2{}^{16}O}$, and $D_{H_2{}^{18}O}/D_{H_2{}^{16}O}$ are from *Merlivat* [1978].

Condensation fractionation factors are computed from the following relations [*Merlivat and Nief*, 1967; *O'Neil*, 1968; *Majoube*, 1971]:

$$\ln \alpha_D = [-2.15412T + 706.4594] \times 10^{-3}$$

$$\ln \alpha_{18O} = [1.137 \times 10^6 T^{-2} - 415.6T^{-1} - 2.0667] \times 10^{-3} + 0.003$$

Once the model determines the steady state composition of recondensed vapor for a specified set of conditions, calculation of the resulting isotopic composition of throughfall is accomplished as follows. The amount of snow remaining at end of interception is given by

$$m_t = m_o - m_l = d\rho - tl$$

where $m_t$, $m_o$, and $m_l$ are the mass of snow remaining after interception time $t$, original mass of snow, and mass of snow lost, respectively; $d$ is depth of original snow; $\rho$ is density of original snow and $l$ is the sublimation loss rate per unit area.

The fraction of snow that is recondensed at time $t$ is given by

$$f_r = m_r/m_t = tg/m_t$$

where $m_r$ is the mass of recondensed water after interception time $t$ and $g$ is the rate of condensation. The fraction of original snow remaining at time $t$ is

$$f_o = 1 - f_r$$

Then the isotopic composition of the remaining snow (primed species) at time $t$ is

$$\delta D'_{SNO} = f_r(\delta D_{SNOR}) + f_o(\delta D_{SNO})$$

$$\delta^{18}O'_{SNO} = f_r(\delta^{18}O_{SNOR}) + f_o(\delta^{18}O_{SNO})$$

where the subscripts SNO and SNOR represent original and recondensed snow, respectively. As previously indicated, the enrichment ratio is a useful parameter in describing the results:

$$e_r = e_D/e_{18} = \frac{\delta D'_{SNO} - \delta D_{SNO}}{\delta^{18}O'_{SNO} - \delta^{18}O_{SNO}} \equiv \frac{\Delta\delta D_{SNO}}{\Delta\delta^{18}O_{SNO}}$$

where $e_D$ and $e_{18}$ are the isotopic enrichments in deuterium and oxygen 18, respectively.

## Input Values

The variable choice for model simulations presented here was intended to explore the effect of some of the environmen-

tal conditions expected at the site where throughfall measurements were made. The results were then compared to the range of enrichments and evaporation losses suggested by the intercepted snow samples. Critical variables chosen were (1) snow-temperature profiles, (2) atmospheric water vapor pressure (temperature and relative humidity), (3) isotopic composition of atmospheric water vapor, (4) interception time, and (5) size of snowfall. Variables that are related to model performance are (1) size of time step and (2) cell size. The latter two affect the accuracy of the result in the same way that any numerical model simulates a continuous process using discrete computational steps. Experience has shown that a step size of $10^{-3}$ to $10^{-2}$ s and cell sizes of 0.2 to 1.0 cm are adequate for modeling of snowpacks using observed environmental conditions. See the section on cell size and amount of evaporation for further considerations regarding choice of cell size.

The model accepts a temperature profile as one of the input variables, which remains constant for the time modeled. Time-variant temperature profiles cannot be modeled with the present version of the computer code. For comparison of model results with environmental data, the choice of input variables was made on the basis of limited observations of snow-temperature profiles and atmospheric water vapor isotopic compositions. The choice of values for the various input parameters is discussed below.

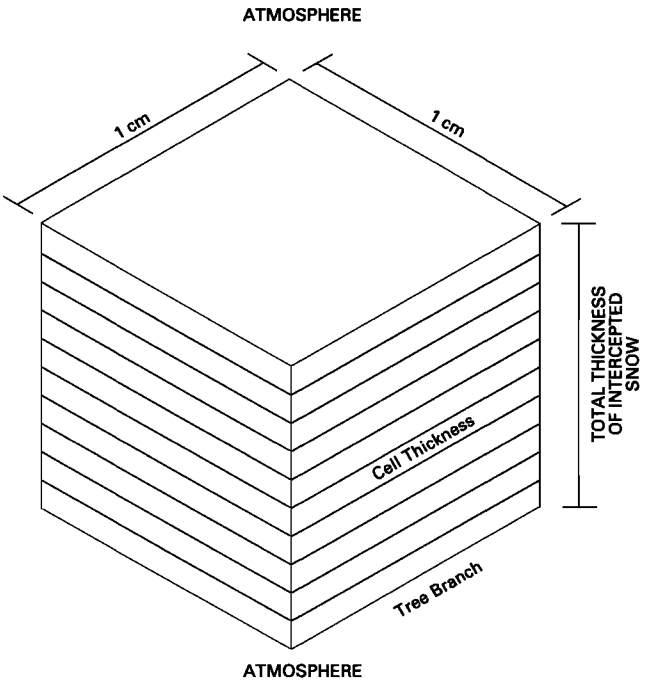


**Figure 8.** Unit cell used in modeling isotope changes occurring in intercepted snow.

### Temperature Profiles of Intercepted Snow and Atmospheric Variables

Figures 5 and 6 show measured temperature profiles for what is believed to be typical midwinter conditions. Examination of these temperature profiles indicates the following. Nighttime conditions suggest that in-snow linear gradients of about 0.4°C/cm or step gradients of about 1°C/cm are likely. Air temperatures lag or lead snow temperatures by as much as about 5°C.

Daytime conditions affect snow temperature profiles dramatically under clear sky conditions, less dramatically in overcast. Clear sky, maximum insolation conditions appear to produce local gradients as high as 2°C/cm for at least short periods of time. Air temperature lag or lead of 9°C appears possible. For purposes of illustration, 13 temperature profile conditions were chosen and are shown in Figure 9. Nighttime humidity often peaks at about 85% and drops to about 35% during the day when clear sky conditions prevail (Figure 10), about 65% under overcast, and may remain between 80 and 90% during snowfall (Figure 10) (H. C. Claassen, U.S. Geological Survey, unpublished data, 1992). Based on the foregoing, the relative humidity values indicated were chosen for the example calculations.

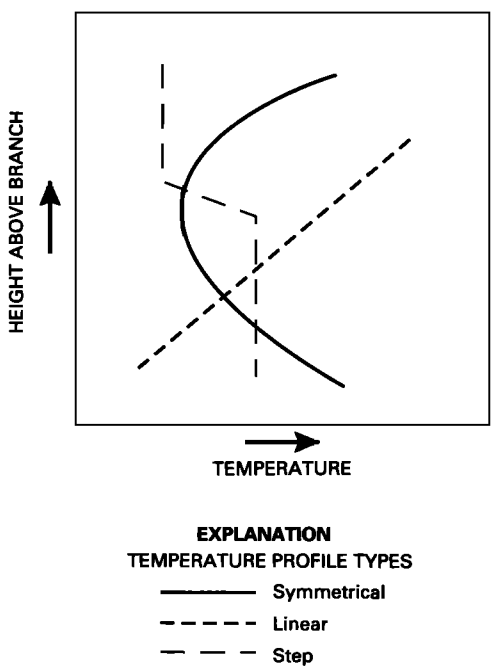


**Figure 7.** Generalized temperature profile types.

### Atmospheric Water Vapor Isotopic Composition

Numerous atmospheric water vapor samples were obtained by the method of *Claassen and Halm* [1992] to establish the range of values that might contact intercepted snow. This method uses cryogenic separation of water vapor from a pumped air sample and was demonstrated to be nonfractionating. From these data a typical midwinter value ($\delta^{18}O_{vapor} = -35‰$; $\delta D_{vapor} = -259‰$) was chosen for most of the calculations. Variations from this value were determined using a regression developed from the vapor composition data and are noted where appropriate.

### Incident Snowfall Isotopic Composition

From the on-site data a typical midwinter value of $\delta^{18}O_{SNO} = -19‰$, $\delta D_{SNO} = -142‰$ was determined for use in simulations.

### Permeability

Snow permeability measurements were reported by *Shimizu* [1970] and *Sommerfeld and Rocchio* [1989]. Although the reported values range widely, a reasonable mean for new snow is $5 \times 10^{-5}$ cm$^2$. As is demonstrated in the appendix, fluxes are

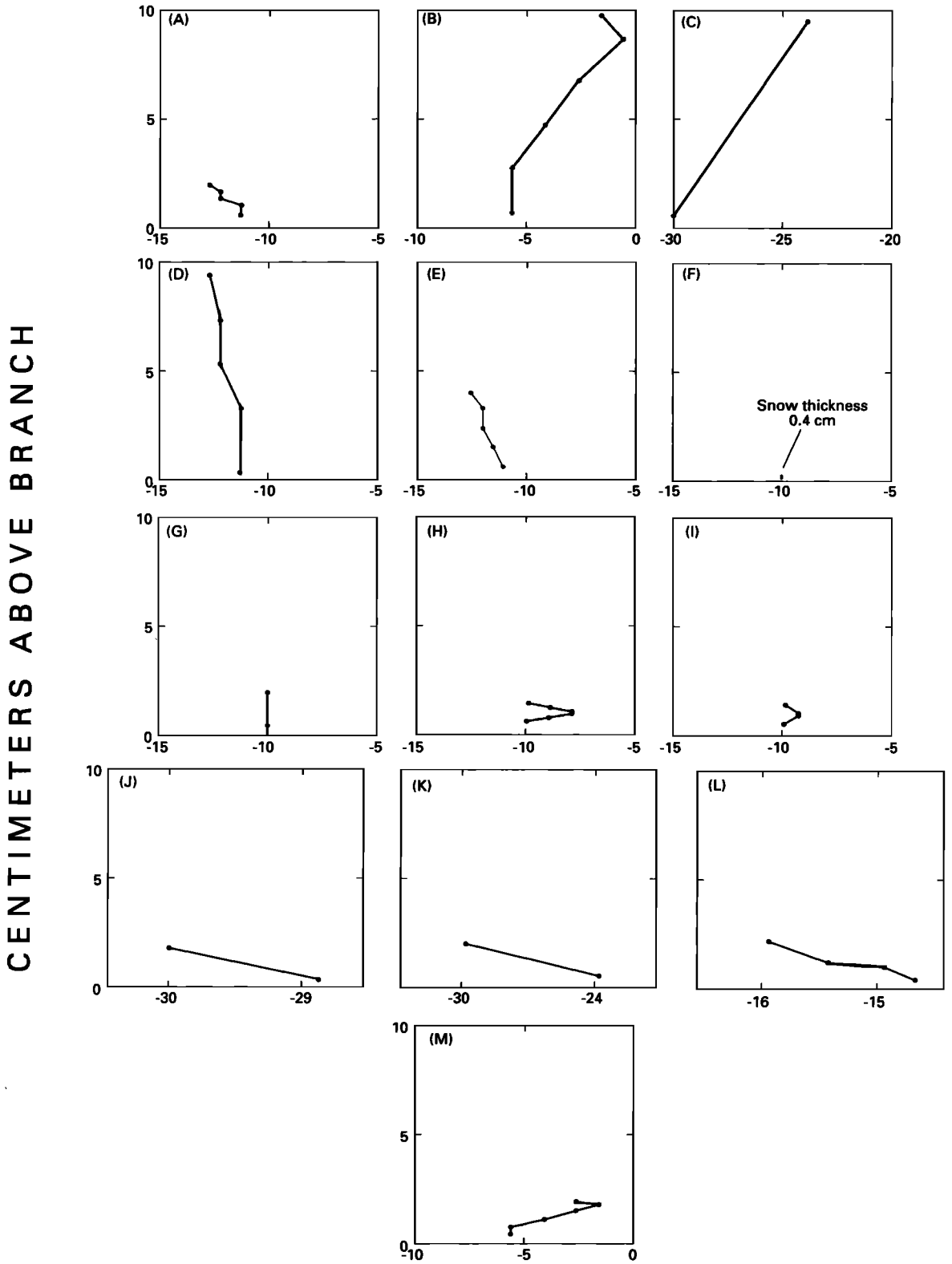


**Figure 9.** Temperature profiles used in model simulations of isotope changes occurring in intercepted snow.

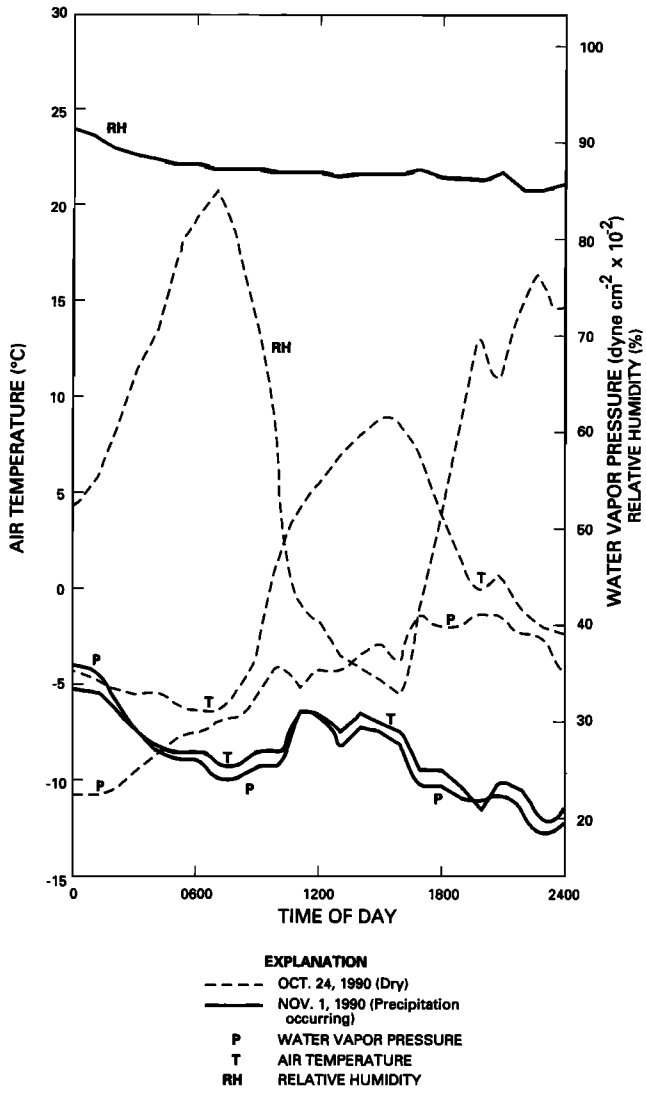


**Figure 10.** Diurnal variation of water vapor pressure, air temperature, and relative humidity on two typical winter days at Snowshoe Mountain.

not strongly dependent on permeability for systems with large permeability, such as freshly fallen snow.

## Results

Model results should simulate the range observed in samples with respect to the following variables: (1) amount of evaporation for reasonable interception times, (2) enrichment in D and $^{18}O$, and (3) enrichment ratio.

### Cell Size and Amount of Evaporation

The rate of evaporation is determined by the snow-to-atmosphere vapor pressure gradient. This gradient is formed by differences in temperature and relative humidity between snow and atmosphere and the cell size chosen. Cell size functions to discretize the snow temperature gradient but also determines the size of the diffusion layer that controls the rate of evaporation loss from snow to atmosphere. Therefore the choice of cell size is not arbitrary but should be related to anticipated environmental conditions that determine diffusion layer dimension. *Merlivat and Coantic* [1975] applied various diffusion layer theories to the evaporation of water by using isotopic analysis of water vapor in wind tunnel experiments. They present data and analysis that relate wind speed to diffusion layer thickness. Their data suggest that a diffusion layer thickness of about 1 cm is reached as wind speed approaches zero (wind curve, Figure 11). For the mean annual wind speed in forest clearings at Snowshoe Mountain, 0.45 m s$^{-1}$, a diffusion layer thickness of 0.85 cm may be estimated. Of course, periodic gusts, even in forest, may be higher than the average. Although somewhat arbitrary, an upper wind speed of 2.5 m s$^{-1}$ (equivalent to a diffusion layer thickness of 0.2 cm) was chosen for the simulations. An illustration of the effect of diffusion layer thickness on evaporation loss may be seen by comparing simulations 3 and 4, or 11 and 12 (Table 1), and by studying Figure 11. Simulations 3 and 4, or 11 and 12, differ only in choice of cell size (diffusion layer thickness) (0.2 and 1.0 cm, respectively) and show the larger evaporation loss associated with the smaller cell size (higher wind speed). Figure 11 suggests that these cell sizes correspond to mean wind speeds of about 2.5 and 0.45 m s$^{-1}$, respectively, and the data in Table 1 (or Figure 11) show the higher evaporation amounts associated with the higher wind speeds. The simulated snow sublimation amounts shown in Table 1 suggest that the model can reproduce the observed amounts.

### Deuterium and Oxygen Isotope Changes

**Range of enrichment.** Modeling results suggest that the amount of enrichment that occurs during interception is controlled primarily by the size of snowfall and interception time, although all the previously stated variables have some effect. It should be evident that for a given set of environmental conditions, viscous and diffusive flux to the atmosphere is nearly the same for a large snowpack as for a smaller one. A small snowpack will lose a greater fraction of mass while condensing amounts of vapor similar to a larger snowpack and therefore will reflect a larger enrichment. Simulations 5, 6, and 7 (Table 1) allow comparison of snow surface losses (simulation 5) relative to losses that may be affected by internal gradients in larger snowpacks (simulations 6, 7). Simulation 5 is a two-cell, 0.4-cm snowfall with no internal gradient and therefore represents evaporation losses driven only by the vapor pressure gradients present at the snow surface. These gradients are determined by the atmospheric vapor pressure, the snow boundary layer vapor pressure(s), and the choice of cell size. Simulation 6 represents a 2-cm snowfall with a minimal internal temperature gradient; simulation 7 represents a 2-cm snowfall with a larger internal gradient. Comparison of absolute evaporation losses for all three simulations reveals no differences (data not shown), although the relative loss is proportionally greater for the smaller snowfall of simulation 5. Increased enrichments, however, are determined by increased internal temperature gradients as shown by the larger enrichment shown in simulation 7 over that in simulation 6 and in simulation 16 over that in simulation 4.

Warm conditions, generally found just prior to the end of interception, produce large losses and large enrichments (simulation 13).

Interception time and cell size may be independently varied to produce similar evaporation losses. Simulations 14 and 15 demonstrate that this does not result in similar enrichments.

Interception time also determines how much snow is lost and how much vapor is condensed within the snowpack. Rel-

ative losses and condensation become larger for the smaller snowfalls, and consequently, the amount of enrichment is larger. For example, compare the results of simulations 1 and 2 with 3 and 4 in Table 1. Absolute enrichments in simulation 1 or 2 are much greater because the initial amount of snow is smaller than that used in simulation 3. Comparison between simulations 3 and 4 suggest that much of the enrichment results from the increased evaporation (13% versus 3%) induced by the larger snow-to-air vapor pressure gradient (defined by choice of 0.2-cm cell size) used in simulation 3. Another comparison to illustrate the relative enrichment effects on small versus large snowpacks may be made using simulations 8 and 9. Here the internal temperature gradients are the same (0.6°C $cm^{-1}$; remember that the top and bottom of snow are similar and the mirror image of a profile produces the same result), but the gradient from the snow surface to the atmosphere must necessarily be different because one snow surface temperature in simulation 8 is −28.8°C and in simulation 9 is −24°C.

Examples that illustrate temporal changes in enrichment of D and $^{18}O$ are found in Figures 12 and 13. Ambient conditions are specified in the figure captions, and snow temperature profiles simulated are shown in Figure 9. As the amount of snow evaporated increases, the fraction of enriched, recondensed vapor becomes larger, resulting in a nonlinear increase in overall snow enrichment. For example, in Figure 12, simulations at 75% relative humidity shov. that at about 2 days interception, 45% of the snow is evaporated and the snow has become enriched about 4.5‰ in D and about 0.5‰ in $^{18}O$; at about 3 days interception, 62% of the snow is evaporated and the snow has become enriched about 10.6‰ in D and about 1.3‰ in $^{18}O$.

**Range of enrichment ratios.** Enrichment ratio has been defined and is a convenient parameter to differentiate the processes that determine the isotopic result of the interception processes. These processes include (1) inward diffusion during periods of high humidity or large and rapid changes in air temperature and (2) variations in atmospheric water vapor composition.

Figures 14 and 15 illustrate short-term changes in the enrichment ratio of condensed vapor that occur while the described systems reach steady state composition of the condensed vapor. As expected, the first vapor to condense is the equilibrium value for the snow temperature profile specified. As diffusion and viscous flow proceed, changes in enrichment ratio from the equilibrium value occur until the steady state value is reached at about 1000 s. The ambient relative humidity has a significant effect on enrichment ratio, especially at higher values where the atmospheric water vapor pressure approaches or exceeds the vapor pressure in the snow. Compare the 75% relative humidity curve using temperature profile A with the 80% curve (Figure 14) or the 75% relative humidity curve with the 81% curve in Figure 15. Enrichment ratios increase significantly in both examples from around 5–8 at 75% relative humidity to 13–14 at the higher humidity. Note also that at low humidity, enrichment ratio is not strongly affected by a change in temperature profile. Compare temperature profiles A and B at 30% relative humidity in Figure 14 (enrichment ratios at steady state about 3.9 and 3.3, respectively). In contrast, at 75% relative humidity, changing the temperature profile from that illustrated by A to B results in significant changes in steady state enrichment ratios of condensed vapor (about 7.8 to about 3.7, respectively). Not illustrated is the result that occurs when

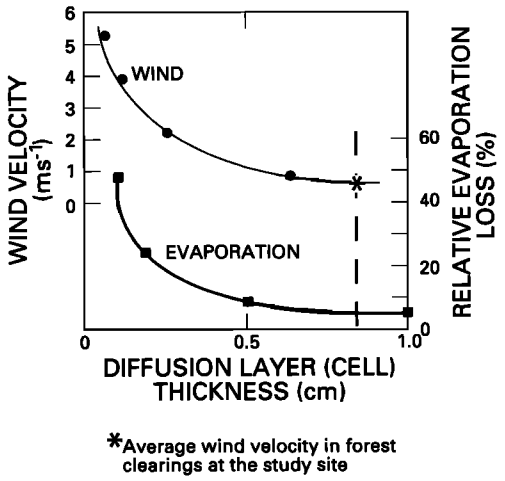


**Figure 11.** Relation of wind speed and evaporation to diffusion layer (cell) thickness.

the atmospheric vapor pressure significantly exceeds the snow vapor pressure. This will be discussed subsequently.

The examples above represent the steady state result of an unvarying set of environmental conditions. Realistically, environmental conditions will continuously vary, sometimes dramatically, as illustrated in Figures 5 and 6, which are selected examples of on-site measurements. Ordinarily, vapor pressure gradients are toward the atmosphere, by virtue of the higher relative humidity that exists within the snow. Occasionally, the temperature difference between snow and atmosphere is large enough (atmosphere higher) or the atmospheric relative humidity is large enough to produce a vapor pressure gradient reversal. Because atmospheric vapor is considerably lighter isotopically than vapor ordinarily within the intercepted snowpack, any condensation of this vapor occurring in the snow would result in the snow's becoming isotopically lighter. The effect of outward diffusion combined with varying periods of inward diffusion is illustrated in Figure 16. In this instance, outward diffusion results in snow having an enrichment ratio of 5.0. An increase in atmospheric relative humidity from 45 to 75% produces an inward diffusing condition. If this condition persists for 5% of the interception time, snow enrichment having an enrichment ratio of about 9 results; if 8% of the time, an enrichment ratio of 15 will result. A second example is given in Figure 17 where the snow profile is warmer and a larger fraction of inward diffusing condition is required to result in a particular enrichment ratio.

Nominal isotopic compositions were chosen for atmospheric water vapor and snow. Deviations from these values will affect enrichment ratios. Figures 18a and 18b illustrate the effect of varying $\delta D_{AIR}$ and $\delta^{18}O_{AIR}$ from the nominal value chosen and the effect of variations in $\delta D_{SNO}$ and $\delta^{18}O_{SNO}$ on enrichment ratios.

## Model Limitations and Discussion of Results

As is frequently the case when modeling complex environmental systems, many simplifying assumptions have been relied on to develop an algorithm for sublimation of intercepted snow. Some of these assumptions have been previously mentioned; the more important are discussed below, with an assessment of their impact on overall results.

**Table 1.** Results of Selected Model Simulations

| Simulation Number and Profile* | Snow Depth, cm | Interception Time, days | Cell size | Ambient Air Temperature, °C | Ambient Relative Humidity, % | Snow Loss, % | Recondensed Vapor Composition, ‰ | | Final Snow Composition, ‰ | | Enrichment, ‰ | | Enrichment Ratio, dimensionless |
|---|---|---|---|---|---|---|---|---|---|---|---|---|---|
| | | | | | | | $\delta D_{SNOR}$ | $\delta^{18}O_{SNOR}$ | $\delta D'_{SNO}$ | $\delta^{18}O'_{SNO}$ | $\Delta\delta D$ | $\Delta\delta^{18}O$ | |
| 1A | 2 | 1 | 0.2 | −10.5 | 68 | 33 | −92.2 | −10.03 | −139.4 | −18.52 | 2.63 | 0.47 | 5.55 |
| 2A | 2 | 2 | 0.2 | −10.5 | 68 | 66 | −92.2 | −10.03 | −131.5 | −17.12 | 10.45 | 1.88 | 5.55 |
| 3D | 10 | 2 | 0.2 | −10.5 | 68 | 13 | −86.8 | −9.62 | −141.8 | −18.97 | 0.18 | 0.03 | 5.88 |
| 4D | 10 | 2 | 1.0 | −10.5 | 68 | 2.7 | −86.5 | −9.69 | −141.8 | −18.97 | 0.16 | 0.03 | 5.96 |
| 5F | 0.4 | 0.1 | 0.2 | −10 | 50 | 48 | ... | ... | −142.0 | −19.00 | 0 | 0 | ... |
| 6I | 2 | 0.1 | 0.2 | −10 | 50 | 9.6 | −48.1 | +6.48 | −142.0 | −19.00 | <0.01 | <0.01 | 3.69 |
| 7H | 2 | 0.1 | 0.2 | −10 | 50 | 9.6 | −46.0 | +7.96 | −141.9 | −18.97 | 0.12 | 0.03 | 3.56 |
| 8J | 2 | 5 | 0.2 | −30 | 50 | 75 | −0.7 | +13.06 | −141.4 | −18.87 | 0.56 | 0.13 | 4.41 |
| 9C | 10 | 5 | 0.2 | −30 | 50 | 24 | +5.4 | +16.12 | −141.8 | −18.94 | 0.24 | 0.06 | 4.20 |
| 10K | 2 | 5 | 1.0 | −30 | 50 | 24 | −27.5 | +6.05 | −135.8 | −17.63 | 6.25 | 1.37 | 4.57 |
| 11G | 2 | 0.1 | 1.0 | −10.5 | 50 | 2.0 | ... | ... | −142.0 | −19.00 | 0 | 0 | ... |
| 12G | 2 | 0.1 | 0.2 | −10.5 | 50 | 9.9 | ... | ... | −142.0 | −19.00 | 0 | 0 | ... |
| 13M | 2 | 0.75 | 0.2 | −3 | 68 | 68 | −106.5 | −10.64 | −128.8 | −15.89 | 13.19 | 3.11 | 4.24 |
| 14E | 4.25 | 14 | 0.85 | −10.5 | 68 | 51 | −88.6 | −9.49 | −136.0 | −17.93 | 5.97 | 1.06 | 5.60 |
| 15E | 4.25 | 7 | 0.425 | −10.5 | 68 | 51 | −88.5 | −9.42 | −138.9 | −18.45 | 3.07 | 0.55 | 5.59 |
| 16B | 10 | 4 | 1.0 | −10 | 68 | 31 | −63.0 | +3.69 | −139.1 | −18.16 | 2.93 | 0.84 | 3.48 |

Three dots indicate no data.

*Snow temperature profiles are given in Figure 9 (profile A appears in Figure 9a, profile B in Figure 9b, etc.). Each simulation assumed snow density of 0.1; permeability of $5 \times 10^{-5}$ cm$^2$; original snowfall isotopic composition is $\delta D_{SNO} = -142$; $\delta^{18}O_{SNO} = -19$; ambient air moisture isotopic composition is $\delta D_{AIR} = -259$, $\delta^{18}O_{AIR} = -35$.

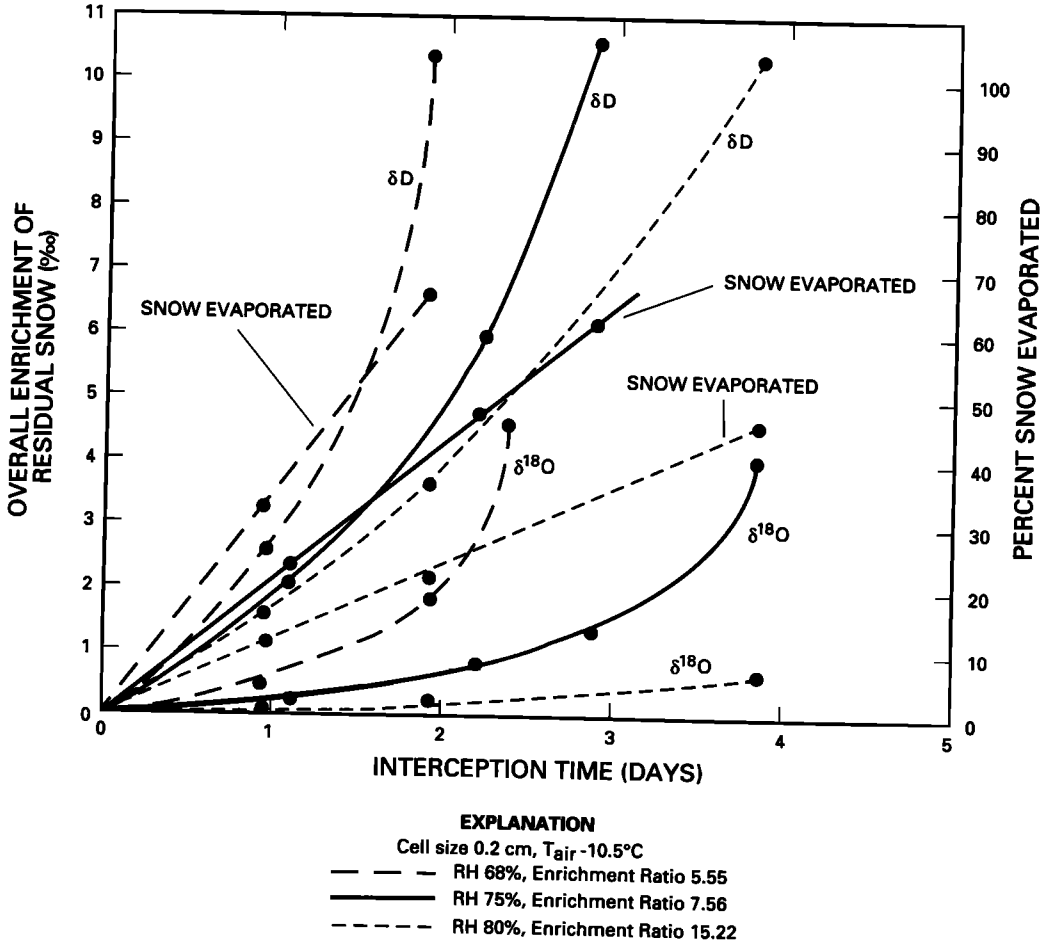


**Figure 12.** Simulated changes in isotopic composition of snow during sublimation of 2-cm snowfall with temperature profile A (Figure 9a).

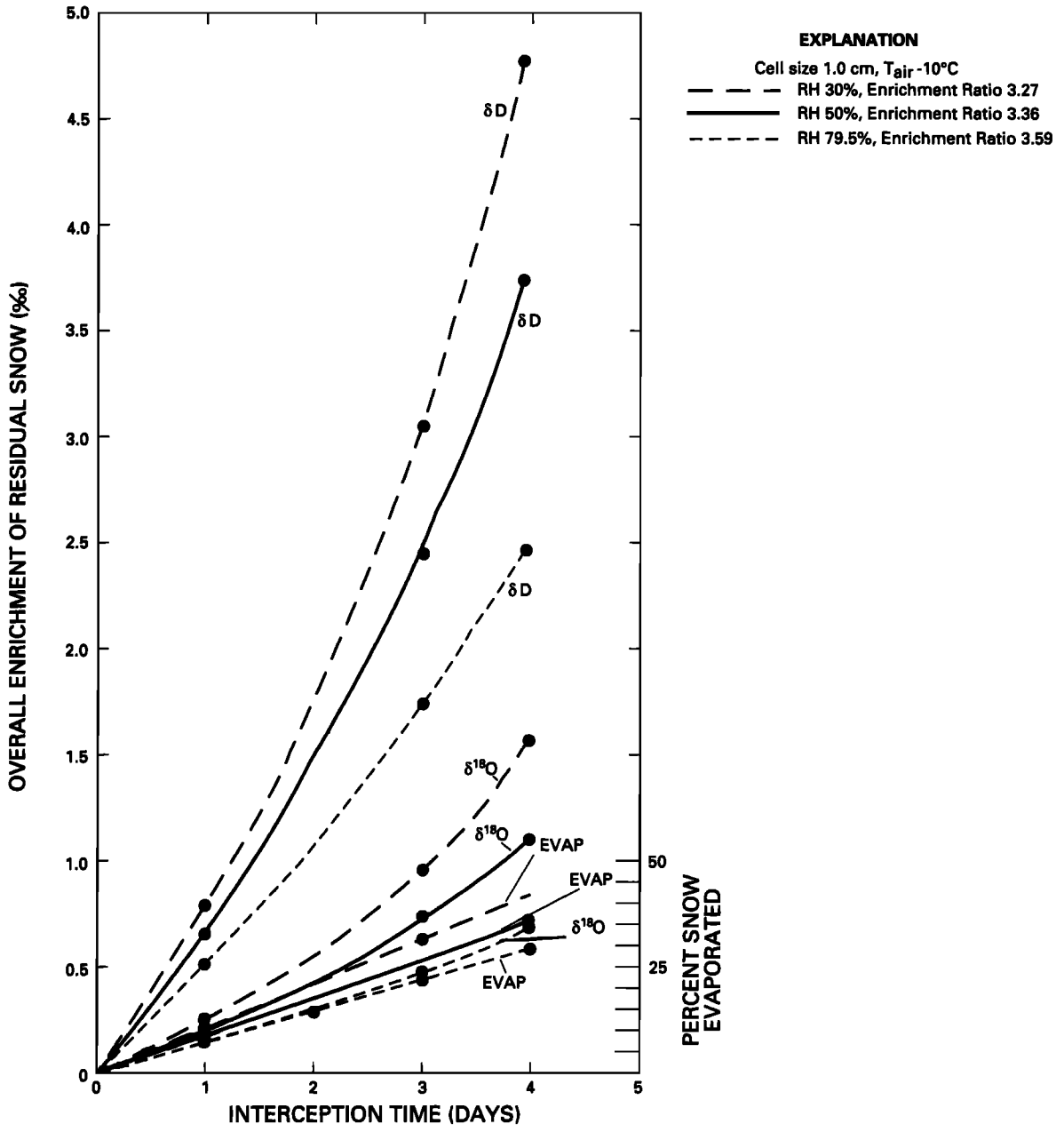


**Figure 13.** Simulated changes in isotopic composition of snow during sublimation of 10-cm snowfall with temperature profile B (Figure 9b).

In its present form the model assumes all intercepted snow initially has a single isotopic composition; therefore the probability that snowfall composition changes during a storm or that intercepted snow comprises multiple snowfalls is not addressed. It is expected that results would not be qualitatively different from those obtained assuming snow homogeneity because changes in isotope composition are influenced primarily by factors other than initial snow composition.

Temperature and humidity profiles are assumed constant during sublimation. Time-variable temperature profiles and variable atmospheric humidity would be computationally more complex, but the results are expected to lie within the milieu of results heretofore presented, because time-variable profiles may be viewed as linear combinations of time-constant profiles.

Sublimation of only original snow is assumed. The effect of resublimation of condensed vapor is more difficult to evaluate than the effects of temperature, relative humidity, and initial snow composition. A microphysical model of the distribution of condensed vapor within the intercepted snow would aid development of an appropriate algorithm. Studies of snow metamorphosis are valuable, but determining the relative amounts of original snow and modified snow available for subsequent sublimation would be difficult, if a physical analog is desired. As discussed earlier, very little effect on final composition should be seen, except at large sublimation losses. The appropriate form of the algorithm at large sublimation loss remains obscure at this time.

Given the above assumptions a protocol was established to demonstrate that the model could simulate the range of results obtained from analysis of on-site samples and data.

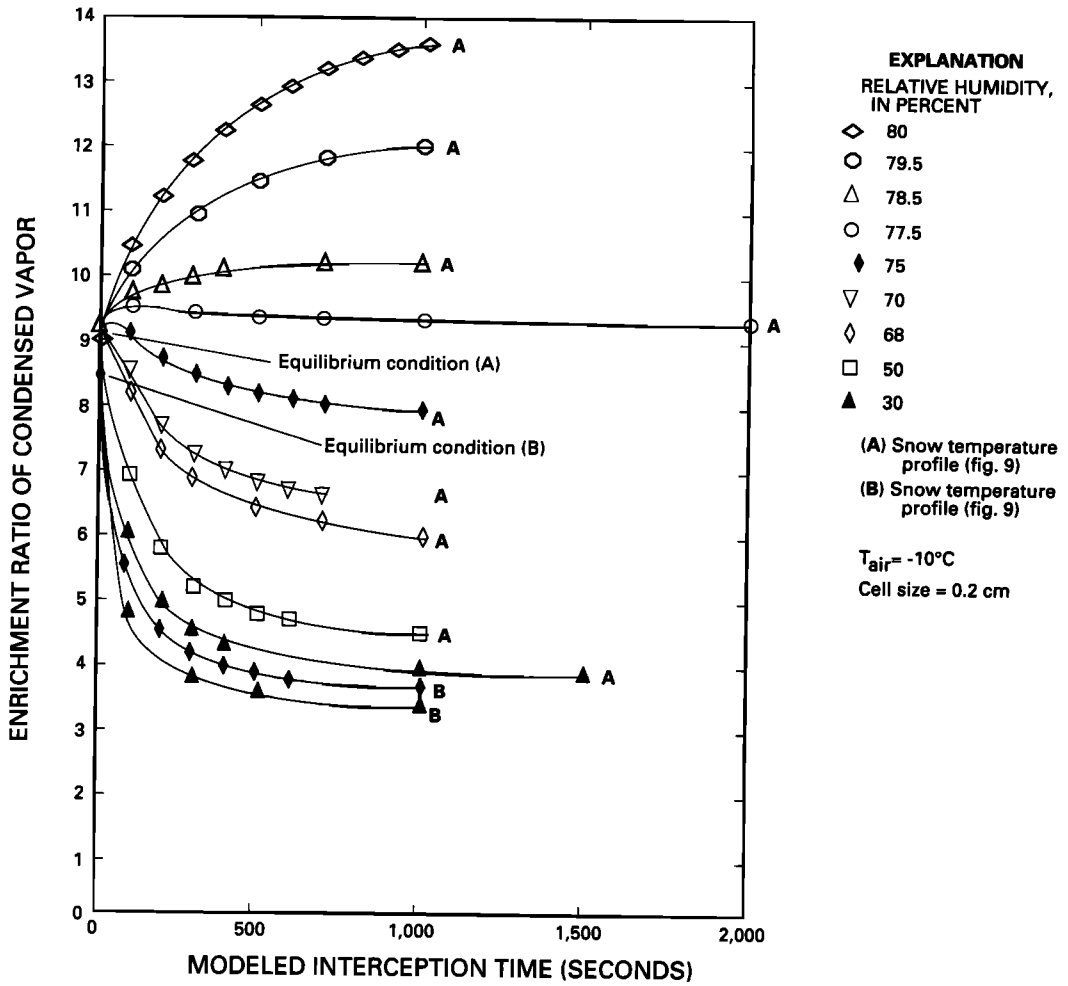


**Figure 14.** Simulated changes with time in enrichment ratio as affected by ambient relative humidity.

Ideally, data collected from an individual, instrumented branch for a known interception period should be compared to simulation results; however, this has not proven practical. The model is entirely based on vapor fluxes and does not address the energy balance for the intercepted snow. Although the energy balance of snow in a forest is extremely complex, estimates of winter solstice incident radiation and snow albedo indicate that sufficient radiation can be absorbed to account for the vapor fluxes computed using the model presented [*Leonard and Eschner*, 1968].

The conditions chosen for illustration of the interrelation of variables were suggested by the limited on-site data. Model runs demonstrated that the range of enrichment ratios observed in throughfall (Figure 3) can be simulated by various combinations of outward and inward diffusing conditions (see Figures 14–17 and Table 1). The absolute enrichments are increased by either longer interception times (see Figures 12 and 13) or smaller snowfalls (Table 1), and the range observed in the on-site data can be simulated.

Whereas the modeled isotopic results may be compared to on-site data only, modeled sublimation amounts are examined in the following discussion.

Examination of data from seven winter seasons (October–May) indicates that the average snowfall event is about 0.4 cm of water equivalent, or about 4 cm of snow depth. Combined with snowfall frequency data, it is determined that about 9 cm of snow falls in a week. This snow will be exposed on evergreens to a much larger extent than it would be had it merely fallen on unvegetated ground. Thus the overall evaporation rate of intercepted snow is larger than that of snow on ground. The model accounts for one of the effects, two-sided exposure of the snow on branchlets. The model does not account for the increased exposure that results from the irregular catch of snowfall by the trees. Observation of snow interception on Engelmann spruce branches reveals that not all branchlets are covered, even at high loading. In contrast, bridging of snow between branchlets, and even branches, occurs at greater snow loadings.

Two approaches were taken to estimate the increased snow exposure during interception over that which occurs on unvegetated ground. One is a simple geometric argument. A representation of an evergreen as a conical section with major axis 4 times the minor axis suggests an eightfold surface area increase over that of the horizontal (ground) area covered. This geometric argument probably exaggerates the surface area increase because the tree is not a solid whose entire surface is available for snow interception. It may be safely assumed, however, that the increase in evaporation surface may be in the vicinity of 800%.

Another approach is to use leaf area index estimates (LAI, the total surface area of foliage per unit ground area) to approximate the increased snow exposure area resulting from

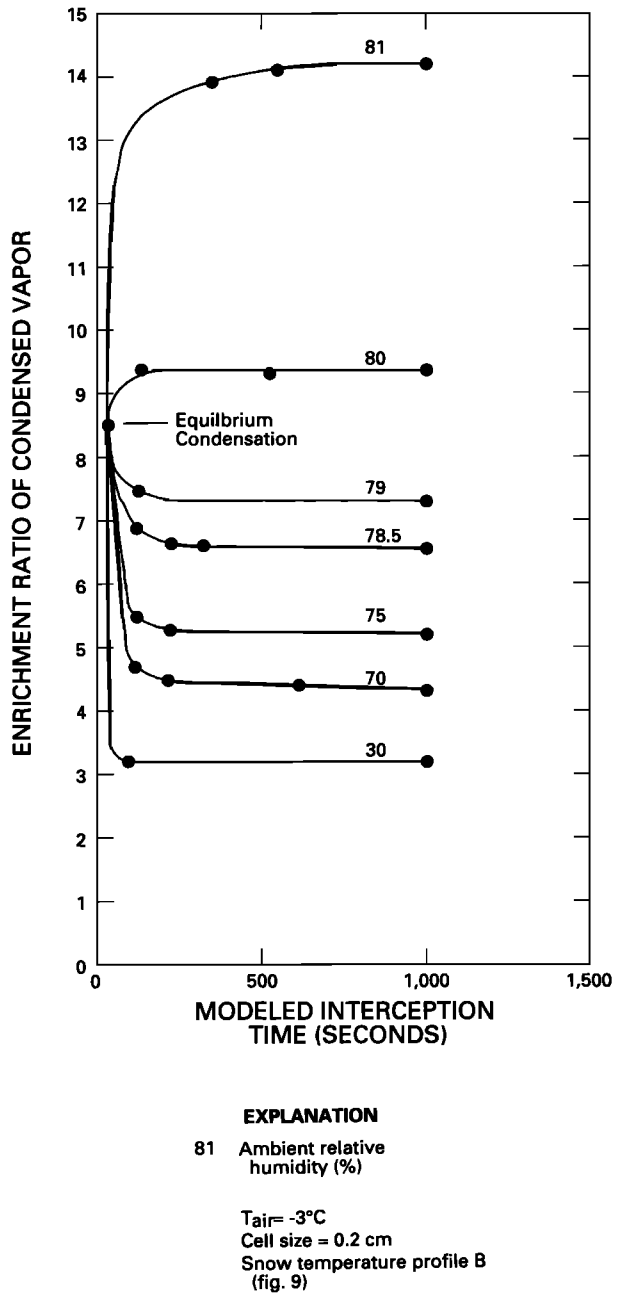


**Figure 15.** Simulated changes with time in enrichment ratio as affected by ambient relative humidity.

interception. LAI measurements of a Douglas fir stand, which has similar configuration to Engelmann spruce, showed LAI values around 8 [*Marshall and Waring*, 1986]. Because not all leaves (branches) are covered, and because bridging occurs, it is not known whether the effective exposure area is greater or less than LAI.

Measured loss rates (Figure 2) indicate that, on average, one-half the snow is lost. To evaluate whether modeled snow loss rates are consistent with on-site observations and measurements made at other locations by other means, the following comparisons were made. Estimates of winter snow loss from the Wagon Wheel Gap, Colorado, forested watershed (on Snowshoe Mountain), reported by *Bates and Henry* [1928], result in a value of 0.075 cm $d^{-1}$ for the entire watershed. Interception losses were estimated at 0.027 cm $d^{-1}$, with about 20% of the watershed covered by evergreens. Although the density of evergreens of *Bates and Henry* [1928] cannot be assessed, it may be inferred that the interception loss rate for evergreens is greater than twice the nonforested rate and would be about 0.135 cm $d^{-1}$. *Bergen and Swanson* [1964] and *Slaughter* [1970] reported nonforested winter evaporation values for another Colorado site that were approximately one-eighth the values for the forested site at Snowshoe Mountain. Model simulations over a broad range of conditions yield results for loss rates from branchlets of less than 0.01 to 0.08 cm $d^{-1}$, which would project to forested area rates of from 0.08 to 0.64 cm $d^{-1}$, if we assume the increased surface exposure area is about a factor of 8, evaporation is proportional to surface area, and snow is present on branchlets the entire winter season. Average loss rates determined from the on-site data are 0.080 cm $d^{-1}$ for dense evergreen forest and should represent a realistic upper limit for the site climatic regime. It may be concluded that simulations yield results consistent with on-site observations.

## Summary and Conclusions

A conceptual and computational model is presented that describes the sublimation losses and hydrogen and oxygen isotope composition of throughfall in a high-altitude spruce forest in southwestern Colorado. The model treats the intercepted snowpack as a temperature-heterogeneous porous medium that allows viscous and diffusive fluxes to flow according to water vapor pressure gradients. These gradients are induced by time-dependent changes in ambient air temperature, relative

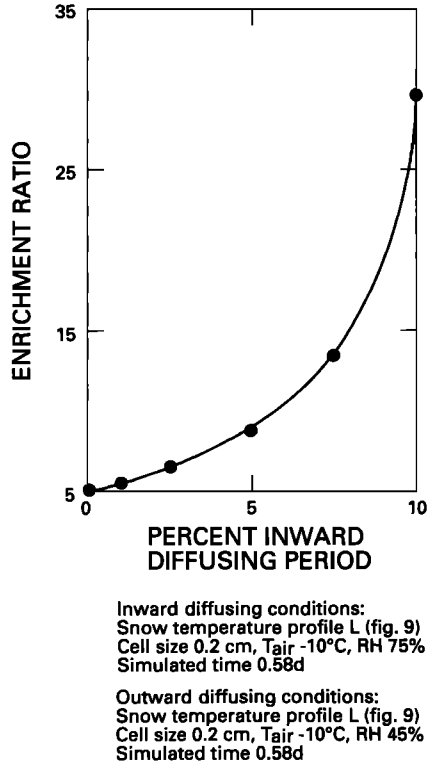


**Figure 16.** Simulated changes in enrichment ratio caused by varying relative amounts of inward diffusing atmospheric water vapor and using snow temperature profile L (Figure 9l).

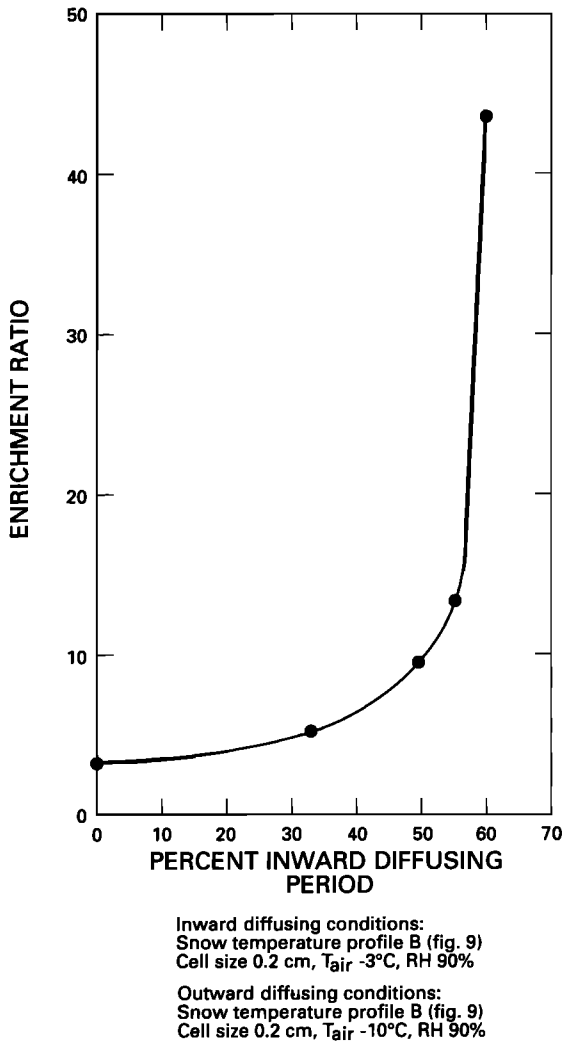


**Figure 17.** Simulated changes in enrichment ratio caused by varying relative amounts of inward diffusing atmospheric water vapor and using snow temperature profile B (Figure 9b).

humidity, and variations in insolation. Variables considered in the model include permeability for determination of viscous flux; ambient air temperature, humidity, and isotopic composition; snow isotopic composition; and snowpack humidity and temperature profile. Model simulations were made using snow profile temperature data obtained on site in addition to a range of anticipated environmental conditions. The results of these simulations mirror the range of observations of isotopic enrichment undergone by intercepted snow. Simulated sublimation loss rates compare favorably with on-site measurements and values reported in the literature for climatic regimes similar to the site.

Assumptions of constant temperature and humidity profiles and initially homogeneous snow composition may be made more realistic by (1) algorithm modification, (2) more extensive on-site observations of temperature and humidity profiles, (3) sequential sampling of snowfall for isotopes during storms, and (4) accurate measurements of interception time. The above could be combined with synoptic sectioning of intercepted snowpacks from various tree locations. Results from laboratory studies, where controlling variables may be regulated, may be compared to model output. The effects of snow interception should also be studied in climatic regimes different from Snowshoe Mountain.

Exclusive of the validity of the model to explain and predict changes in isotopic composition of intercepted snow, one may speculate on isotopic modification of recharge brought about by the observed enrichment of throughfall. For example, consider a heavily forested watershed climatically similar to Snowshoe Mountain. If this densely canopied forest comprises 75% area coverage and if sublimation losses from snowpack on the ground are ignored, overall isotopic modification may be estimated. For Snowshoe Mountain climatic conditions the isotopic modification of winter snowpack would be $\Delta\delta^{18}O = 1.3‰$, $\Delta\delta D = 7.8‰$. If this were the only isotopic modification to precipitation prior to recharge, the climatic interpretation would suggest a climate that was 2.6°C warmer than if no isotopic enrichment had occurred ($1.3‰/0.5‰°C^{-1}$). It may be concluded that isotopic modification of intercepted snow should be considered in interpreting the relation between precipitation and soil water and groundwater isotopes.

## Appendix: Gas Flux in Porous Media

In the general case for very permeable media such as snow, Knudsen diffusion and slip flux may be ignored, and the Stefan-Maxwell equations are used to determine the relative importance of the viscous and diffusive fluxes of water vapor in the snow [*Thorstenson and Pollock*, 1989]. The pertinent relations for a two-component system of air and water vapor follow, all from *Thorstenson and Pollock* [1989] with minor modifications.

$$N^T = N^D + N^V \tag{1}$$

where $N^T$, $N^D$, and $N^V$ are the total, diffusive and viscous gas fluxes of all species present. If the diffusion regime is assumed to be molecular, the Stefan-Maxwell equation may be expressed as follows [see *Thorstenson and Pollock*, 1989, equation (79)]

$$\frac{\chi_{H_2O}N^T_{AIR} - \chi_{AIR}N^T_{H_2O}}{D_{H_2O/AIR}} = \frac{P_{ATM}\nabla\chi_{H_2O}}{RT} \tag{2}$$

where $\chi$ is the mole fraction, $\nabla\chi$ is the mole fraction gradient, $D$ is the binary molecular diffusivity, $P_{ATM}$ is the atmospheric total pressure, $R$ is the gas constant, and the subscripts refer to the gas species present in the binary system: air and water vapor.

Assuming

$$N^T_{AIR} = 0$$

one obtains by substitution and rearrangement of (2)

$$N^T_{H_2O} = \frac{P_{ATM}\nabla\chi_{H_2O}D_{H_2O/AIR}}{\chi_{AIR}RT} \tag{3}$$

By introducing Darcy's law and relating the intrinsic Klinkenberg parameter $b_m$ to the permeability of the medium $B_K$, *Thorstenson and Pollock* [1989, equation (70)] derive an expression for the total viscous flux:

$$N^V = \frac{N^T_{H_2O}M^{1/2}_{H_2O}}{(\mu_{AIR}b_m/P_{ATM}) + \chi_{H_2O}M^{1/2}_{H_2O} + \chi_{AIR}M^{1/2}_{AIR}} \tag{4}$$

where $M$ is the molecular weight and $\mu$ is the viscosity of the specified gas. But [*Thorstenson and Pollock*, 1989, equation (63)]

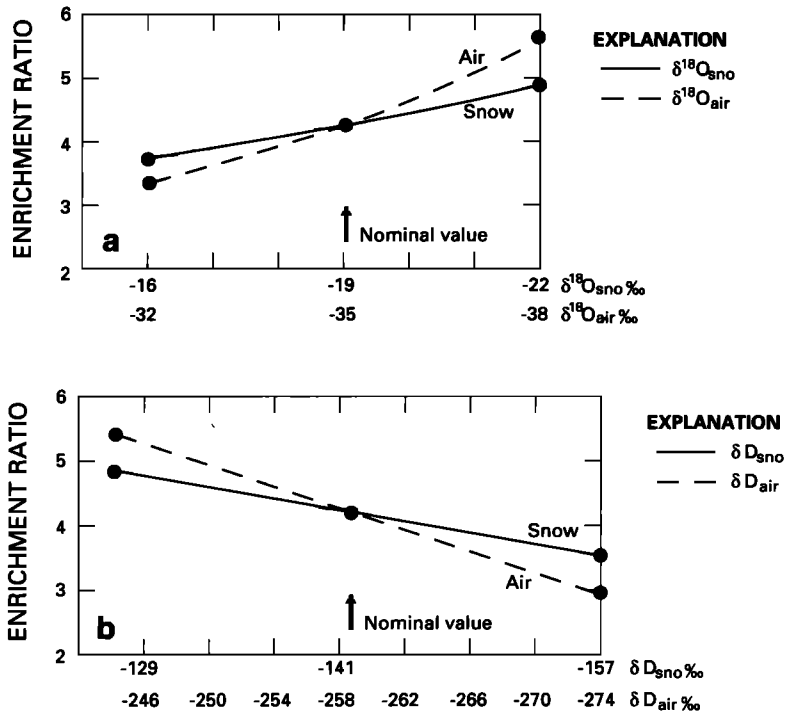


**Figure 18.** (a) Effect on enrichment ratio of varying oxygen isotope composition of air and snow from the nominal value used in most simulations. Conditions held constant: Temperature profile B, 2-cm snow, $T_{AIR} = -3°C$, $\delta D_{AIR} = -259$, $\delta D_{SNO} = -142$. (b) Effect of enrichment ratio of varying deuterium composition of air and snow from the nominal value used in most simulations. Conditions held constant are the same as in Figure 18a.

$$b_m = b_{AIR} M_{AIR}^{1/2} / \mu_{AIR} \tag{5}$$

where $b_{AIR}$ is the measured Klinkenberg parameter for air, and [*Thorstenson and Pollock*, 1989, equation (69)] (modified for the units used in this paper)

$$b_{AIR} = 39.909 B_k^{-0.39} \tag{6}$$

By substituting (5) and (6) into (4) we obtain

$$N^V = \frac{N^T_{H_2O} M^{1/2}_{H_2O}}{39.909 B_k^{-0.39} M^{1/2}_{AIR} / P_{ATM} + \chi_{H_2O} M^{1/2}_{H_2O} + \chi_{AIR} M^{1/2}_{AIR}} \tag{7}$$

Equation (7) allows calculation of the total viscous flux in the snow from known values of the variables. The viscous flux of water vapor is then obtained from

$$N^V_{H_2O} = \chi_{H_2O} N^V \tag{8}$$

The total diffusive flux is obtained from (1), recalling that it was assumed that $N^T_{AIR} = 0$:

$$N^D = N^T - N^V = N^T_{H_2O} - N^V \tag{9}$$

Then

$$N^D_{H_2O} = N^T_{H_2O} - \chi_{H_2O} N^V \tag{10}$$

The molar water vapor flux arising from molecular diffusion is [*Thorstenson and Pollock*, 1989, equations (74) and (77)]

$$J_{H_2O} = N^D_{H_2O} - \chi_{H_2O} N^D \tag{11}$$

The molar water vapor flux arising from diffusion calculated using Fick's first law [*Thorstenson and Pollock*, 1989, equation (84)] is

$$J^{Fick}_{H_2O} = -P_{ATM} D_{H_2O/AIR} \nabla \chi_{H_2O} / RT \tag{12}$$

Examination of the foregoing equations reveals several facts pertinent to the relative water vapor fluxes in snow. First, the total water vapor flux is significantly determined by the vapor pressure gradient (equation (3)), which in the snow is determined by the temperature gradient and in the atmosphere by temperature and relative humidity. Second, the viscous flux of water vapor is only weakly dependent on permeability (equations (7) and (8)) until the permeability drops to about $10^{-7}$ cm$^2$ (10 darcy). As permeability decreases, the term that contains permeability in (7) becomes larger. It becomes greater than 2% of the sum of the other two terms in the denominator when permeability is decreased to $10^{-7}$ cm$^2$. Thus for larger permeabilities $N^V$ is a constant, and $N^V_{H_2}O$ depends primarily on $\chi_{H_2O}$ per (8). Larger viscous fluxes in the snow would therefore be associated with warmer snow temperatures.

Two examples are given to demonstrate the relative contributions of viscous and diffusive fluxes to water vapor flux. The first example represents typical near-surface conditions where [*Shimizu*, 1970; *Sommerfeld and Rocchio*, 1989]

$$P_{ATM} = 6.8 \times 10^5 \text{ dyn cm}^{-2} \qquad T_{AIR} = T_{SNO} = 253°K$$

$$RH = 0.75 \qquad B_k = 10^{-5} \text{ cm}^2$$

The last value is from *Shimizu* [1970] and *Sommerfeld and Rocchio* [1989]. Also,

$$D_{H_2O/AIR} = 0.194 \text{ cm}^2 \text{ s}^{-1} \qquad \chi_{H_2O} = 1.309 \times 10^{-3}$$

$$\nabla\chi_{H_2O} = 3.68 \times 10^{-4} \text{ cm}^{-1}$$

Then

$$N^T_{H_2O} = -2.311 \times 10^{-9} \qquad N^V = -1.814 \times 10^{-9}$$

$$N^V_{H_2O} = -2.374 \times 10^{-12} \qquad N^D_{H_2O} = -2.309 \times 10^{-9}$$

$$J_{H_2O} = -2.308 \times 10^{-9} \qquad J^{Fick}_{H_2O} = -2.308 \times 10^{-9}$$

Therefore the water vapor flux is 99.9% diffusive and 0.1% viscous under these conditions, and the Fick's law approximation to molecular diffusion flux is valid.

The second example represents conditions that may be found within the intercepted snow during maximum midwinter insolation:

$$P_{ATM} = 6.8 \times 10^5 \text{ dyn cm}^{-2} \qquad T_{AIR} = 263°\text{K}$$

$$\text{RH} = 0.50 \qquad T_{SNO} = 270°\text{K} \qquad B_k = 10^{-5} \text{ cm}^2$$

$$D_{H_2O/AIR} = 0.216 \text{ cm}^2 \text{ s}^{-1} \qquad \chi_{H_2O} = 4.454 \times 10^{-3}$$

$$\nabla\chi_{H_2O} = 1.695 \times 10^{-3} \text{ cm}^{-1}$$

Then

$$N^T_{H_2O} = -1.129 \times 10^{-8} \qquad N^V = -8.864 \times 10^{-9}$$

$$N^V_{H_2O} = -3.948 \times 10^{-11} \qquad N^D_{H_2O} = -1.125 \times 10^{-8}$$

$$J_{H_2O} = -1.124 \times 10^{-8} \qquad J^{Fick}_{H_2O} = -1.124 \times 10^{-8}$$

In this instance, the water vapor flux is 99.6% diffusive and 0.4% viscous, and the Fick's law approximation to molecular diffusion is valid. Decreasing the permeability to $10^{-6}$ cm$^2$ decreases the portion of viscous flux to 0.3%.

## Notation

Dimensions are $M$, mass; $L$, length; $t$, time; and $T$, absolute temperature.

$\alpha_D$ $R_{HDO}$ liquid/$R_{HDO}$ vapor (dimensionless).
$\alpha_O$ $R_{H_2{}^{18}O}$ liquid/$R_{H_2{}^{18}O}$ vapor (dimensionless).
$b$ Klinkenberg parameter, measured using specified gas $i$ ($ML^{-1}t^{-2}$).
$b_m$ intrinsic Klinkenberg parameter, characteristic of the porous medium ($M^{1/2}$ mol$^{-1/2}$ $t^{-1}$).
$B_k$ permeability ($L^2$).
$C_i$ molecular concentration of specified gas $i$ (molecules $L^{-3}$).
$d$ depth of snow at beginning of interception ($L$).
$D_i$ binary molecular diffusivity of specified gas $i$ ($L^2$ $t^{-1}$).
$e_D$ isotopic enrichment of HDO (per mil).
$e_{18}$ isotopic enrichment of $H_2{}^{18}O$ (per mil).
$f$ fraction (dimensionless).
$g$ rate of water vapor condensation per unit area ($Mt^{-1}$).
$J_i$ molar flux of specified gas arising from molecular diffusion (mol $L^{-2}$ $t^{-1}$).
$J^{Fick}_i$ molar flux of specified gas $i$ calculated using Fick's law (mol $L^{-2}$ $t^{-1}$).
$l$ sublimation loss rate per unit area ($Mt^{-1}$).
$m_l$ mass of snow per unit area lost to atmosphere after interception time $t$ ($M$).
$m_o$ original mass of snow per unit area at beginning of interception ($M$).
$m_r$ mass of recondensed water vapor per unit area after interception time $t$ ($M$).
$m_t$ mass of snow per unit area after interception time $t$ ($M$).
$M_i$ molecular weight of specified gas $i$ ($M$ mol$^{-1}$).
$N_{AV}$ Avogadro's number (molecules mol$^{-1}$).
$N^D_i$ total molar diffusive gas flux across a specified boundary of gas $i$ (no subscript denotes all gases) (mol $L^{-2}$ $t^{-1}$).
$N^T_i$ total molar gas flux across a specified boundary of gas $i$ (no subscript denotes all gases) (mol $L^{-2}$ $t^{-1}$).
$N^V_i$ total molar viscous gas flux across a specified boundary of gas $i$ (no subscript denotes all gases) (mol $L^{-2}$ $t^{-1}$).
$P_{ATM}$ ambient atmospheric pressure ($ML^{-1}$ $t^{-2}$).
$P_i$ vapor pressure of specified water vapor isotope $i$ ($ML^{-1}$ $t^{-2}$).
$P_{H_2O}$ total water vapor pressure ($ML^{-1}$ $t^{-2}$).
$P_{H_2O(eq)}$ total water vapor pressure in equilibrium with ice ($ML^{-1}$ $t^{-2}$).
$R$ gas constant ($ML^2$ $t^{-2}$ $T^{-1}$ mol$^{-1}$).
RH relative humidity (dimensionless decimal fraction).
$R_{HDO} = C_{HDO}/C_{H_2{}^{16}O}$ (dimensionless).
$R_{H_2{}^{18}O} = C_{H_2{}^{18}O}/C_{H_2{}^{16}O}$ (dimensionless).
$R_{SMOW\ HDO} = 1.5576 \times 10^{-4}$.
$R_{SMOW\ H_2{}^{18}O} = 2.0052 \times 10^{-3}$.
$t$ time.
$T$ absolute temperature ($T$).
$T_{AV}$ average absolute temperature between pair of cells ($T$).
$\chi_i$ mole fraction of specified gas $i$ (dimensionless).
$\nabla\chi_i$ mole fraction gradient of specified gas ($L^{-1}$).
$\delta D = [(R_{HDO}/R_{SMOW\ HDO}) - 1] \times 10^3$ (per mil).
$\delta^{18}O = [(R_{H_2{}^{18}O}/R_{SMOW\ H_2{}^{18}O}) - 1] \times 10^3$ (per mil).
$\delta D_{SNO}$, $\delta^{18}O_{SNO}$ isotopic value of snowfall at beginning of interception (per mil).
$\delta D'_{SNO}$, $\delta^{18}O'_{SNO}$ isotopic value of intercepted snow at interception time $t$ (per mil).
$\delta D_{SNOR}$, $\delta^{18}O_{SNOR}$ isotopic value of recondensed vapor at interception time $t$ (per mil).
$\Delta\delta D$, $\Delta\delta^{18}O$ change in isotopic value resulting from sublimation of snow (per mil).
$\rho$ density of snow at beginning of interception ($ML^{-3}$).
$\mu_i$ viscosity of specified gas $i$ ($ML^{-1}$ $t^{-1}$).

## References

Bader, H., R. Haefeli, E. Bucher, I. Neher, O. Eckel, and C. Thams, Der Schnee und seine Metamorphose, *Beitr. Geol. Schweiz, Geotech. Ser., Hydrol., 3*, 1939. (English translation, Snow and its metamorphism, *Transl. 14*, Snow, Ice, and Permafrost Res. Estab., Hanover, N. H., 1954.)

Bates, C. G., and A. J. Henry, Forest and stream flow experiment at Wagon Wheel Gap, Colorado, *Mon. Weather Rev., 56*, suppl. 30(1), 79 pp., 1928.

Bergen, J. D., and R. H. Swanson, Evaporation from a winter snowcover in the Rocky Mountain forest zone, in Proceedings of the 32nd Annual Western Snow Conference, pp. 52–58, Nelson, B. C., Canada, 1964.

Bird, R. B., W. E. Stewart, and E. N. Lightfoot, *Transport Phenomena*, 780 pp., John Wiley, New York, 1960.

Claassen, H. C., and D. R. Halm, Design and validation of an on-site atmospheric water-vapor sampling system for hydrogen- and oxygen-isotope analysis, *U.S. Geol. Surv. Open File Rep., 92-74*, 1992.

Claassen, H. C., M. M. Reddy, and D. R. Halm, Use of chloride ion in determining hydrologic basin water budgets—A three year case study in the San Juan Mountains, Colorado, *J. Hydrol., 85*, 49–71, 1986.

Colbeck, S. C. (Ed.), *Dynamics of Snow and Ice Masses*, 468 pp., Academic, San Diego, Calif., 1980.

Colbeck, S. C., Air movement in snow due to wind pumping, *J. Glaciol., 35*(120), 209–213, 1989.

Craig, H., and L. I. Gordon, Deuterium and oxygen-18 variations in the ocean and marine atmosphere, in *Stable Isotopes in Oceanographic Studies and Paleotemperatures*, edited by E. Tungiorgi, Consiglio Nazionale delle Ricerche, p. 9–130, Rome, 1965.

Craig, H., L. I. Gordon, and Y. Horibe, Isotopic exchange effects in the evaporation of water, 1, Low temperature experimental results, *J. Geophys. Res., 68*, 5079–5087, 1963.

Davis, R. E., J. Dozier, and A. T. C. Chang, Snow property measurements correlative to microwave emission at 35 GHz, *IEEE Trans. Geosci. Remote Sens., GE-25*(6), 751–775, 1987.

DeHoff, R. T., Quantitative serial sectioning analysis, *J. Microsc., Oxford, 131*, 259–263, 1983.

de Quervain, M., Snow structure, heat and mass flux through snow, in *Proceedings of the International Symposium on the Role of Snow and Ice in Hydrology, 1972*, vol. 2, pp. 203–226, UNESCO, Paris, 1973.

Dorsey, N. E., *Properties of Ordinary Water-Substance*, Reinhold, New York, 1940.

Dozier, J., R. E. Davis, and R. Perla, On the objective analysis of snow microstructure, in Avalanche Formation, Movement and Effects, *IAHS Publ. 162*, 49–59, 1987.

Eisenberg, D., and W. Kauzmann, *The Structure and Properties of Water*, 296 pp., Oxford University Press, New York, 1969.

Epstein, S., R. P. Sharp, and A. J. Gow, Six year record of oxygen and hydrogen isotope variations in South Pole firn, *J. Geophys. Res., 70*, 1809–1814, 1965.

Friedman, I., C. Benson, and J. Gleason, Isotopic changes during snow metamorphism, in Stable Isotope Geochemistry—A Tribute to Samuel Epstein, *Spec. Publ. Geochem. Soc., 3*, 211–221, 1991.

Fritz, P., and J. C. Fontes, *Handbook of Environmental Geochemistry*, 545 pp., Elsevier, New York, 1980.

Gow, A. J., On the accumulation and seasonal stratification of snow at the South Pole, *J. Glaciol., 5*, 467–477, 1965.

Gray, D. M., and D. H. Male (Eds.), *Handbook of Snow*, 776 pp., Pergamon, New York, 1981.

Hoover, M. D., and C. F. Leaf, Process and significance of interception in Colorado subalpine forest, in *Forest Hydrology*, edited by W. E. Sopper and H. W. Lull, pp. 213–224, Pergamon, New York, 1967.

Judy, C., J. R. Meiman, and I. Friedman, Deuterium variations in an annual snowpack, *Water Resour. Res., 6*, 125–129, 1970.

Leonard, R. E., and A. R. Eschner, Albedo of intercepted snow, *Water Resour. Res., 4*, 931–935, 1968.

Majoube, M., Fractionnement en $^{18}O$ entre la glace et la vapeur d'eau, *J. Chim. Phys. Phys. Chim. Biol., 68*, 625–636, 1971.

Marshall, J. D., and R. H. Waring, Comparison of methods of estimating leaf-area index in old-growth Douglas-fir, *Ecology, 67*, 975–979, 1986.

Merlivat, L., Molecular diffusivities of $H_2{}^{16}O$, $HD^{16}O$, and $H_2{}^{18}O$ in gases, *J. Chem. Phys., 69*, 2864–2871, 1978.

Merlivat, L., and M. Coantic, Study of mass transfer at the air-water interface by an isotopic method, *J. Geophys. Res., 80*, 3455–3464, 1975.

Merlivat, L., and G. Nief, Fractionnement isotopique lors des changements d'état solide-vapeur et liquide-vapeur de l'eau à des températures inférieures à 0°C, *Tellus, 19*, 122–126, 1967.

Moser, H., and W. Stichler, Deuterium and oxygen-18 contents as an index of the properties of snow covers, in Proceedings of the Grindlewald Symposium, *IAHS Publ., 114*, 122–135, 1974.

O'Neil, J. R., Hydrogen and oxygen isotope fractionation between ice and water, *J. Phys. Chem., 72*, 3683–3684, 1968.

Rogers, R. R., *A Short Course in Cloud Physics*, 2nd ed., 235 pp., Pergamon, New York, 1979.

Saxena, R. K., Estimation of canopy reservoir capacity and oxygen-18 fractionation in throughfall in a pine forest, *Nord. Hydrol., 17*, 251–260, 1986.

Schytt, W., *Glaciology II—Norwegian-British-Swedish Antarctic Expedition 1949–1952*, vol. 4, *Scientific Results*, 148 pp., Norsk Polarinstitutt, Oslo, 1958.

Seligman, G., *Snow Structure and Ski Fields*, 555 pp., Macmillan, New York, 1936.

Shimizu, H., Air permeability of deposited snow, *Contrib. Inst. Low Temp. Sci., Hokkaido Univ., Ser. A, 22*, 1–32, 1970.

Slaughter, C. W., Evaporation from snow and evaporation retardation by monomolecular films—A review of literature, *Spec. Rep. 130*, 33 pp., U.S. Army Cold Reg. Res. and Eng. Lab., Hanover, N. H., 1970.

Sommerfeld, R. A., and J. Rocchio, The Darcy permeability of fine-grained compact snow, in Proceedings of the 46th Annual Eastern Snow Conference, pp. 121–128, Quebec, Que., Canada, 1989.

Sommerfeld, R. A., C. Judy, and I. Friedman, Isotopic changes during the formation of depth hoar in experimental snowpacks, in Stable Isotope Geochemistry—A Tribute to Samuel Epstein, *Spec. Publ. Geochem. Soc., 3*, 205–209, 1991.

Stewart, M. K., Stable isotope fractionation due to evaporation and isotopic exchange of falling waterdrops: Applications to atmospheric processes and evaporation of lakes, *J. Geophys. Res., 80*, 1133–1146, 1975.

Thorstenson, D. C., and D. W. Pollock, Gas transport in unsaturated zones: Multicomponent systems and the adequacy of Fick's laws, *Water Resour. Res., 25*, 477–507, 1989.

Trabant, D., and C. Benson, Field experiments on the development of depth hoar, *Mem. Geol. Soc. Am., 135*, 3309–3322, 1972.

Troendle, C. A., and R. M. King, The effect of timber harvest on the Fool Creek watershed, 30 years later, *Water Resour. Res., 21*, 1915–1922, 1985.

Whillans, I. M., and P. M. Grootes, Isotopic diffusion in cold snow and firn, *J. Geophys. Res., 90*, 3910–3918, 1985.

H. C. Claassen and J. S. Downey, U.S. Geological Survey, Water Resources Division, MS 412, Box 25046, Denver Federal Center, Denver, CO 80225.

(Received January 25, 1994; revised July 29, 1994;
accepted August 4, 1994.)